Preprints (www.preprints.org) | NOT PEER-REVIEWED | Posted: 13 September 2022 doi:10.20944/preprints202209.0174.v1

Article

Open-source Photovoltaic - Electrical Vehicle Carport Designs

Nicholas Vandewetering [1], Koami Soulemane Hayibo [2] and Joshua M. Pearce [2,3,*]

[1] Department of Civil & Environmental Engineering, Western University, London, ON N6A 3K7, Canada; nvandew@uwo.ca
[2] Department of Electrical & Computer Engineering, Western University, London, ON N6A 3K7, Canada; khayibo@uwo.ca
[3] Ivey School of Business, Western University, London, ON N6A 3K7, Canada
* Correspondence: joshua.pearce@uwo.ca

Abstract:

Solar powering the increasing fleet of electrical vehicles (EV) demands more surface area than may be available for photovoltaic (PV) powered buildings. Parking lot solar canopies can provide the needed area to charge EVs, but are substantially costlier than roof- or ground-mounted PV systems. To provide a lower-cost PV parking lot canopy to supply EV charging beneath them, this study provides a full mechanical and economic analysis on three novel PV canopy systems: (1) exclusively wood, single parking spot spanning system, (2) wood and aluminum double parking spot spanning system, and (3) wood and aluminum cantilevered system for curbside parking. All systems can be scalable to any amount of EV parking spots. The complete designs and bill of materials (BOM) of the canopies are provided along with basic instructions and are released with an open source license that will enable anyone to fabricate them. The results found single-span systems have cost savings of 82%-85%, double-span systems save 43%-50%, and cantilevered systems save 31%-40%. In the first operation year, the PV canopies can provide 157% of energy needed to charge the least efficient EV currently on the market if it is driven the average driving distance in London ON, Canada.

Keywords: open-source; photovoltaic; mechanical design; electric vehicle; solar energy; solar carport; electric vehicle charging station

1. Introduction

Solar photovoltaic (PV) technology, now a long-established sustainable source of electricity [1] has overcome the historic barrier of cost with rapid declines [2]. Today PV electricity generation is often less expensive conventional power sources [3]. Unsurprisingly, PV has driven [4] high penetration of renewable energy into the grid [5]. The growth of low-cost solar is expected to continue in the short term [5].

This is important, because although conventional electric loads are in decline, there is expected to be a growth in in demand [6] due to growth in electric vehicles (EVs) [7]. Like PV, plug-in hybrid electric vehicles (PHEV) are becoming increasingly important as the sales of EVs expands to 2.2% of the global vehicle market [8]. This EV market share is set to expand to 30% by 2040 [9], which is identical to BP's prediction for PV in the same year [10]. The rapid rise of both PV to displace fossil fuels and EV (driving even more electricity demand) presents a challenge to find appropriate surface area [11]. Studies of roof area for PV [12–14] including building integrated PV (BIPV) [15,16] can account for some of the demand [17], however, more than roof surface area is required [18].

One interesting method to kill two birds with one stone is utilize the stranded assets of non-productive parking lot areas as solar farms with solar carports. PV canopies located over parking spaces enabling sustainable electricity production [19–22]. Such solar carports can be used to directly feed electricity to the grid or act as an anchor for a local microgrid[23]. Perhaps most intriguingly, the PV can be used for EV charging as for example they may increase revenue for retail stores [24]. Many studies have already

© 2022 by the author(s). Distributed under a Creative Commons CC BY license.

Preprints (www.preprints.org) | NOT PEER-REVIEWED | Posted: 13 September 2022 doi:10.20944/preprints202209.0174.v1

investigated the design and optimization of solar systems to charge EVs [25] as a core component of sustainable strategy [26]. EVs can be charged at work under such canopies [27–29] and EVs can even be integrated into the grid to overcome intermittency via vehicle-to-grid implementations [30–33]. Even at home using PV and EV charging can create a nanogrid [34]. PV and vehicle to grid appear viable [35–37].

One of the primary reasons that all parking lots are not already covered with PV canopies is the capital costs, which are more expensive than conventional ground-mounted PV as well as roof-mounted PV. This is primarily due to the capital cost of the structure (or racking) for the PV that must be up more than 6 feet above the ground. Current systems are designed almost entirely from galvanized steel or aluminum framing. Many wooden and steel hybrid canopies designed for single car parking, however, are available, and have capital costs as low as $4,995 CAD, but are not approved for PV installation [38–40]. Most of these systems are built at a 5-degree pitch to minimize wind loading, and have a minimum clearance of 2.4 m from the ground [41]. Although adequate for most EVs, this clearance may not be suitable for larger planned EVs in the future [42]. These carport systems typically span 1-2 vehicles before requiring a column, but heavy industrial level carports have been made to span up to 3 vehicles [43]. For example, a single vehicle 4.8 kW system costs $7,230.85 CAD, ($1.51/W) and a 5 kW system costs $6,512.17 CAD ($1.30/W) [44]. A proposed 160 kW projects in Alberta using exclusively aluminum for the carports have structural costs of $230,000 CAD, which equates to $1.43 per W [45]. Thus, typical systems today cost anywhere from $1.30-$1.50 per W.

A recent successful approach to reduce the capital cost of PV racking for ground mounted systems is to design using wood [46,47]. In addition, to substantial cost advantages in North America, wood is sustainable [48], renewable and comprised of approximately half carbon so it can be thought of as a carbon sink [49]. As wood requires relatively low energy processing, wood has a negative combined embodied energy and carbon over alternative materials conventionally used for racking. For example, most PV racking is aluminum and even with a third being recycled material, aluminum has over 5 times the embodied CO_{2e}/kg of wood [50].

Thus, to provide a lower-cost PV parking lot canopy to supply EV charging beneath them, this study provides a full mechanical and economic analysis on three novel PV canopy systems with a 25-year expected lifetime to match a standard PV warranty including: (1) an exclusively wood, single parking spot spanning system, (2) a wood and aluminum double parking spot spanning system, and (3) a wood and aluminum cantilevered system. The designs are presented as 5 stall and 6 stall builds, but all systems are entirely scalable to any amount of parking spots needed. The complete designs and bill of materials (BOM) of the canopies are provided along with basic instructions and are released with an open source license that will enable anyone to fabricate them. The BOM costs are compared to the cost of proprietary commercial PV canopies. The PV that the canopies are able to hold are simulated and the solar energy produced is compared to the average electric load for an EV. The results of this study are discussed in the context of using low-cost PV canopies to provide the necessary electricity to charge EVs.

2. Materials and Methods

2.1 Material Properties

No. 2 SPF pressure-treated lumber and ASTM approved hardware that is easily accessible at typical hardware stores was used for this design. The material properties are summarized in the Vandewetering et al. design [46], and are used for the structural analysis of these systems. These designs carefully follow the guidelines of the National Building Code of Canada (NBCC) [51] and the National Design Specification for wood construction [52] to ensure the structures are safe and serviceable for at least 25 years to match common PV warranties.

6061 T6 aluminum is an exceptional corrosion resistant material with a high strength to weight ratio that is widely available in the retail market. To allow for longer spans that

Preprints (www.preprints.org) | NOT PEER-REVIEWED | Posted: 13 September 2022 doi:10.20944/preprints202209.0174.v1

are beyond the capacity of pressure-treated lumber, two of these systems utilize 6061 T6 aluminum I beams. The mechanical properties, provided by Metal Supermarkets in London [53] used for analysis is summarized in Table 1. For the strength design aluminum, guidelines in the Aluminum Design Code CSA S157-05 [54] are followed.

Table 1. Mechanical Properties of 6061 T6 Aluminum, from Metal Supermarkets, London.

Material Property	Value
Density	2767 kg/m^3
Yield Strength	275 MPa
Ultimate Tensile Strength	310 MPa
Shear Strength	206 MPa
Young's Modulus	68,900 MPa

Using these allowable stress capacities, a structural analysis that is based on system location can be conducted following the steps shown in Appendix A. The general equations and diagrams can be adapted using any design load calculated in the NBCC to ensure the allowable stresses are not exceeded. This process should be carefully followed for other regions to see if the design load must be increased or can be decreased. If there is a significant difference between the applied load and the resisting capacity of any member in the structural analysis, then users can select smaller members and recalculate to save more on material costs. If a structural material capacity found in [46] is exceeded, then the next size up should be chosen and analyzed to ensure adequate capacity.

2.3. Economic Analysis

A detailed economic analysis based on the bill of materials is conducted. The cost of these systems is based on local purchases, and since the system has the potential to be a DIY system, the labor cost is not factored into the base case study. Future work can compare the labor cost differential (if there is any with more conventional racking structures). The comparison between the cost of the different racking systems is done on a per W basis. Since these systems are scalable, a sensitivity analysis is conducted to compare the cost per W of systems of varying sizes. Additionally, since both wood and aluminum are subject to highly varying price fluctuations, sensitivity analyses are conducted on the total system cost based on the commodity prices of the materials they are composed of. Finally, a sensitivity analysis is done to account for the price difference in different locations around the world based on the local availability of the building materials.

2.4. Design Analysis Assumptions

The same design analysis assumptions from the design in [46] were used for this system.

2.5. Electrical Analysis

A realistic energy production, and load matching analysis are performed to evaluate the solar PV installed on the carport's contribution to the charging power of the EV. The System Model Advisor (SAM) software is used in this study for evaluating the energy production of the PV system [55]. SAM is preferred to other PV simulation software because its results are validated with real-world data, and its operation is open source [56]. Furthermore, SAM has access to a large database of weather data from satellite measurements or weather stations. The simulation is run for two locations in North America. London in Ontario, Canada is chosen to represent cold climates with long periods of snow, while Los Angeles is selected as a high-solar flux location that has fewer winter days.

2.5.1. EV Charging Station Load Assumptions

Estimating EV charging station load is challenging because of the variety of EV cars' specifications and charging patterns. On the market, the battery capacity of current EV varies between 16.7 kWh and 118 kWh [57]. At the same time, the charging time can vary depending on the charge voltage, the vehicle user, as well as the location where the vehicle is charging. To standardize EV charging stations' electrical features, the North American

Preprints (www.preprints.org) | NOT PEER-REVIEWED | Posted: 13 September 2022 doi:10.20944/preprints202209.0174.v1

EV charging standards have defined three power levels [58]. The level 1 power charge station has a maximum power level of 1.4 kW, a charging time between 4 and 11 hours, and is suitable for use in homes or offices. The level 2 station is preferred for offices and public parking even though it can be installed in homes. It has a power level of 8 kW and a charging time range of 2 to 6 hours. The power of the level 3 charging station is either 50 kW or 100 kW and is intended for fast-charging large vehicles such as public electrical buses. It has a fast-charging time ranging from 0.4 to 1 hour and 0.2 to 0.5 hours for the 50 kW and 100 kW stations respectively. Other types of charging stations exist, but are vehicle-specific [59].

Despite the power rating of the charging station, the actual power drawn by the EV depends on its charging state. The charging power profile is not constant and varies with the state of charge of the EV, the charging voltage, and the charging current. An EV charging profile, at the base level, has a constant current charging mode followed by a constant voltage charging mode [60,61]. A recent study has proposed a percentage load profile curve for EV users for different charging sites, whether it is home or work, and different days of the week [62]. The load profiles that Zhang et al. used was provided for each gender as well, but for uniformity of the simulation, the average between male and female EV load profiles is used here. The percentage load profile is applied to the charging stations defined by the North American Standard to obtain load profiles in kW. The load profiles are arranged to form a full year of EV load data for the energy simulation in SAM for each type of charging site, with each week consisting of 5 weekdays and 2 weekends. Details the load profile estimation are provided in the study by Zhang et al. [62].

2.5.2. Solar PV Model Assumptions and Simulation

The solar PV energy production is simulated for a year using realistic weather data, real solar PV modules, and real inverter specifications in SAM. The PV energy is simulated for a single carport (15 modules). A single carport is chosen because the results can be scaled proportionally. As per the dimensions of the carport design, each module has an area of 2m by 1m and a power of 410 W_{DC}, accounting for total DC power of 6.15 kW_{DC}. The tilt of the PV modules is constrained by the carport mechanical design tilt of 5°. Optimal orientation of due South (azimuth of 180°) is assumed. The detailed input parameters of the SAM simulation are shown in Table B1 in the appendix.

Due to the complexity of the EV load estimation described previously, two separate simulations are performed. The first simulation focuses on load matching between the proposed PV carport and the different types of charging stations described in Section 2.5.1. The PV simulation is performed hourly, and the results are compared to the EV charging stations load profiles. Specifically, the hourly load profile of the charging stations assuming 24-7 charging of multiple EVs is compared to the hourly energy production for load matching. This is done to provide some insights into the how the PV and EV charging station would interact in time of use rate structures or for systems that would store PV-generated electricity in an onsite battery to ensure full self-consumption for EV charging as a function of type of charger.

In the second simulation, the simplest case where net metering is in effect (meaning that the prosumer pays only for the net energy used on an annual basis) is analyzed for a single carport used to charge a single EV. The annual energy production of the PV and the annual energy demand of the EV are compared to determine whether the PV system's total production can cover the EV demand with the support of the grid. In this second analysis scenario, the analysis is centered around a single EV, not the charging station. The annual energy consumed by a single EV is determined by multiplying the energy efficiency (Wh/km) of the vehicle to the average distance driven per year. For example, in London Ontario, the average annual distance travelled is 16,000 km [63]. To account for the variability of the EV energy efficiencies, a sensitivity analysis is run using the efficiencies from current EVs on the market (between 109 and 295 Wh/km) [64].

Preprints (www.preprints.org) | NOT PEER-REVIEWED | Posted: 13 September 2022 doi:10.20944/preprints202209.0174.v1

3. Results

All three system types were successfully designed and modeled to exceed Canadian building code, and thus has a life expectancy of 25 years, which matches the warranty of the PV modules.

3.1 Single Spanning System

3.1.1 Single Spanning System Bill of Materials

The bill of materials (BOM) of the one span system is shown in Table 2 in Canadian dollars sourced from Copp's Build-All, London, and Metal Supermarkets, London.

Table 2. Single-Span System Bill of Materials

Member Name	Piece[1]	Cost per Piece[2]	Quantity	Cost
Joists	2 x 10 x 14	$53.99	18	$971.82
	2 x 10 x 12	$46.28	9	$416.52
Double 2x12 Beams	2 x 12 x 16	$85.76	12	$1029.12
Beams	2 x 12 x 10	$53.60	4	$214.40
Joist Splice Tie Plate	3 x 5 Mending Plate	$2.25	24	$54.00
Beam Splice Tie Plate	3 x 7 Mending Plate	$2.79	12	$33.48
Lateral Bracing	2 x 10 x 14	$53.99	3	$161.97
Joist to Beam Ties	H1 Hurricane Ties	$2.19	34	$74.46
Posts	6 x 6 x 16	$88.74	12	$1064.88
Post Lateral Diagonals	2 x 4 x 10	$12.82	4	$51.28
Nuts, Bolts, Washers	3/8" x 10"	$4.52	24	$108.48
Screws	2-1/2" Deck Screws (1175/pail)	$38.99	1	$38.99
D10 Nails	1-1/2" Joist Hanger Nails	$4.65	5	$23.25
Module to Joist Connection	¼" x 2-1/2" Carriage Bolt, Nut, and Washer	$1.01	204	$206.04
			Total Cost with No Concrete	$4448.69
Concrete for Posts	30 Mpa Quikrete concrete	$5.55	36 bags	$199.80
			Total Cost:	$4648.49

[1] All lumber is to be pressure treated, and all hardware is to be hot dipped galvanized.
[2] All costs are in Canadian Dollars as of July 13, 2022, before tax.
[4] Cost per connection (1 bolt, 1 nut, 1 washer).

3.1.2 Single Spanning System Assembly Instructions

To begin, 6 x 6 posts are installed 1.2 m into the ground to penetrate the frost line. Footing sizes are to be calculated using Equation A2 in Appendix B. The front and back posts are to be cut into 3.10 m and 3.40 m, respectively. Footings are to be made 1.25 m away from the edge of each parking line as outlined in Figure 1.

Preprints (www.preprints.org) | NOT PEER-REVIEWED | Posted: 13 September 2022 doi:10.20944/preprints202209.0174.v1

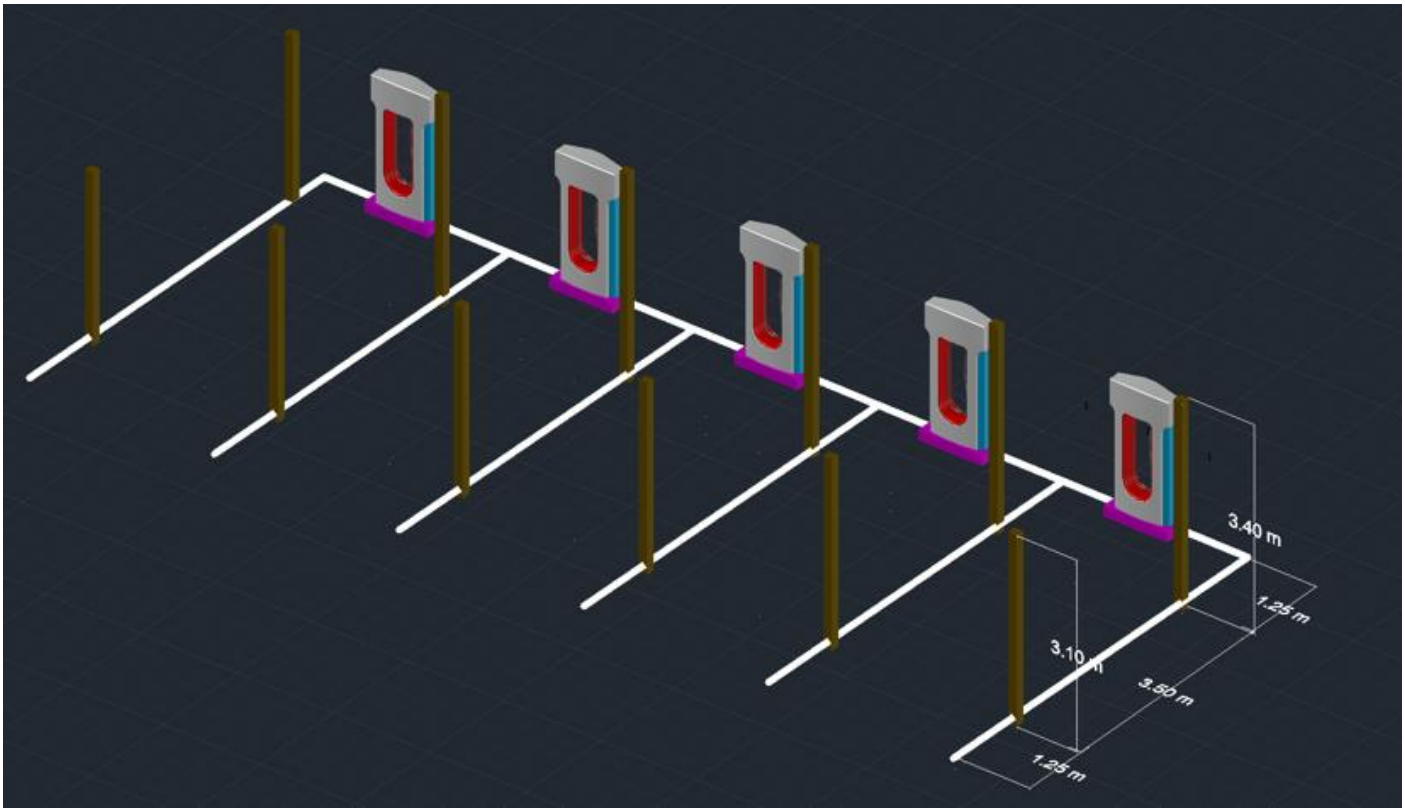

Figure 1. Single-Span System Post Configuration

Then, double 2 x 12 beams are installed onto the posts as shown in Figure 2a. 3/8″ x 10″ galvanized carriage bolts are used for each connection (Figure 2b). To build larger systems, splice joints connect the beams together using mending plates and joist hanger nails (Figure 2c). Splices should be made approximately 20% of a span length away from a post, where the bending moment diagram in Appendix B is roughly 0.

Preprints (www.preprints.org) | NOT PEER-REVIEWED | Posted: 13 September 2022 doi:10.20944/preprints202209.0174.v1

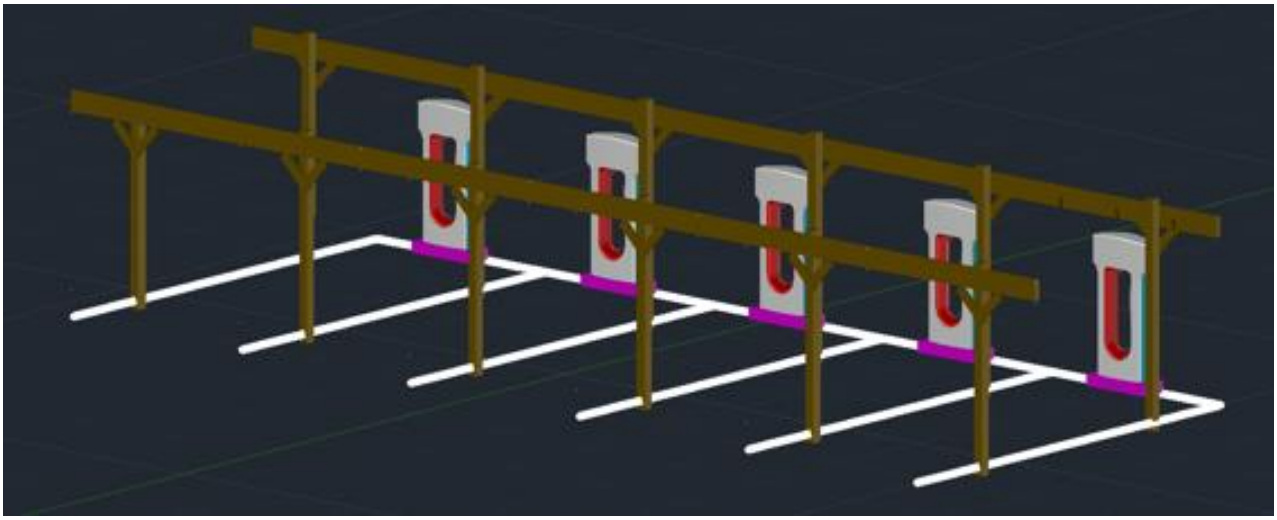

a)

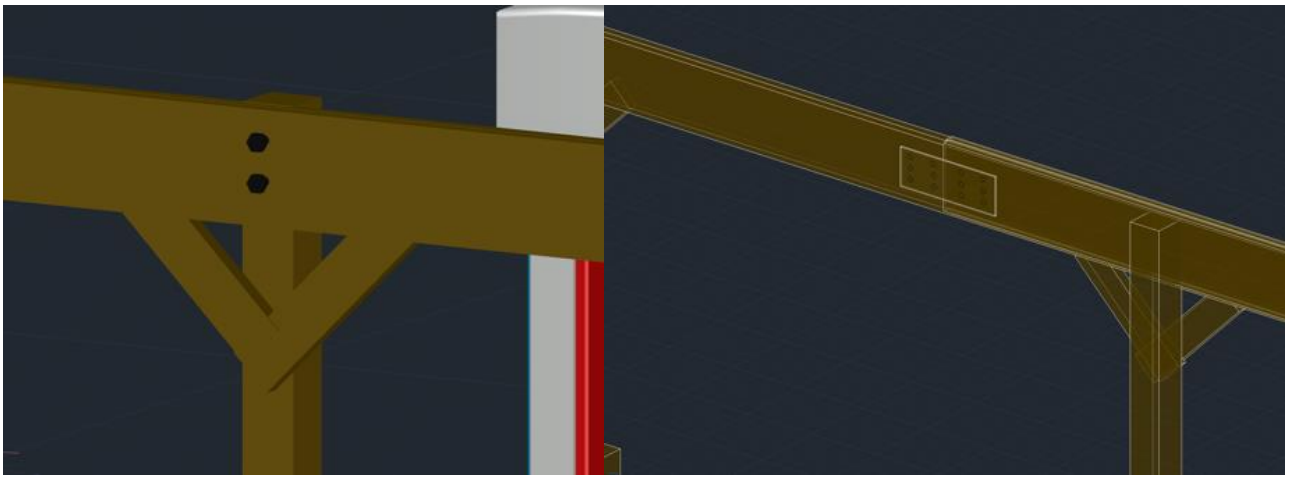

b) c)

Figure 2. Single Span System a) Double 2 x 12 beams installed across posts, b) 2 3/8" carriage bolts, and diagonal 2 x 4 braces per connection, and c) 3 x 5 mending plate with 1-1/2" joist hanger nails to create splice joint at approximately 20% of the span length.

Then, the single 2 x 10 joists are installed with 1 m spacing onto the beams as shown in Figure 3a. Again, splice joints with 3 x 5 mending plates and joist hanger nails are made at 20% of the midspan length. 1 m long 2 x 10s are placed between the joists to serve as lateral bracing. The joists are connected to the beams via H1 hurricane ties as described in Figure 3b.

Preprints (www.preprints.org) | NOT PEER-REVIEWED | Posted: 13 September 2022 doi:10.20944/preprints202209.0174.v1

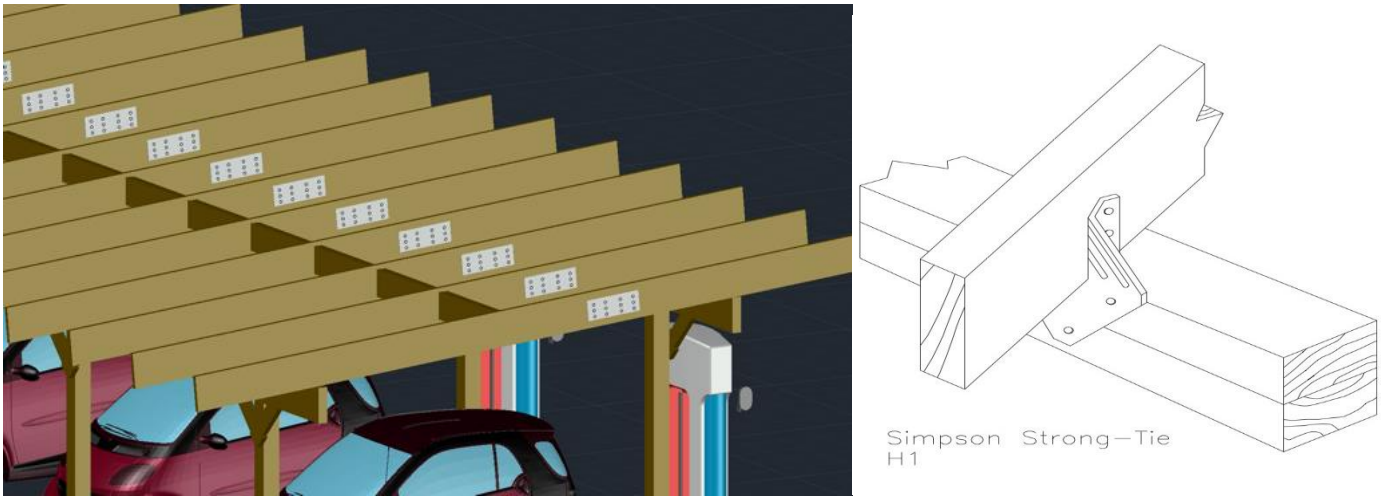

3) b)

Figure 3. Single Span System a) 2 x 10 joists installed along the beams, spaced 1 m apart, connected with splice joints, and braced with 2 x 10 braces, and b) joist to beam installation using H1 hurricane ties.

Modules are installed directly onto the joists with ¼" x 2-1/2" lag screws as shown in the newly proposed Sadat et. al. frame design shown in in Figure 4a, or modules can be installed from the side if they adopt the second Sadat et al. frame design [65] as shown in Figure 4b.

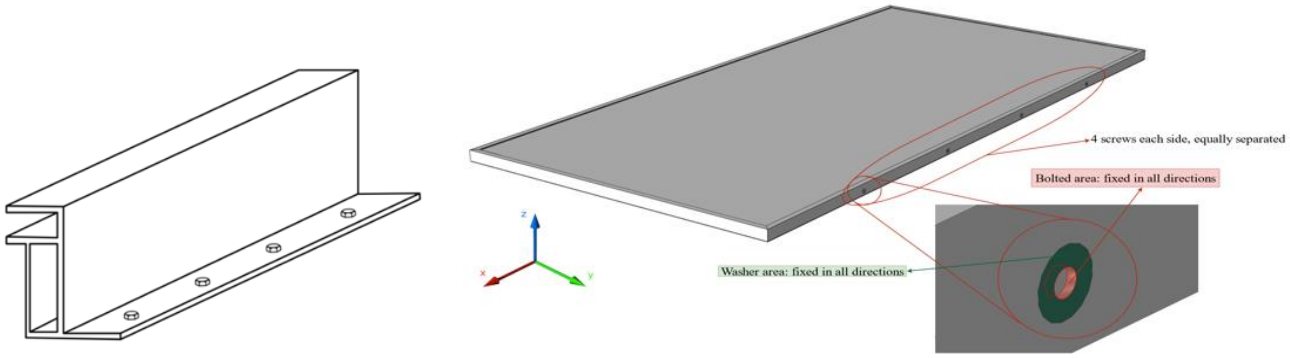

a) b)

Figure 4. a) ¼" x 2-1/2" lag screws connections screwed directly to the top of joists, and b) connections alternatively made to the side of modules into the side of the joists.

If a direct connection cannot be made, extra blocks of wood can be made and installed onto the joists, and carriage bolts, nuts and washers can be installed on the overhanging block as shown in Figure 5.

Preprints (www.preprints.org) | NOT PEER-REVIEWED | Posted: 13 September 2022 doi:10.20944/preprints202209.0174.v1

Figure 5. ¼" x 2-1/2" carriage bolt, nut, and washer used to secure the connection.

The finished system is shown in Figure 6. The system can be disassembled in the reverse manner it was built.

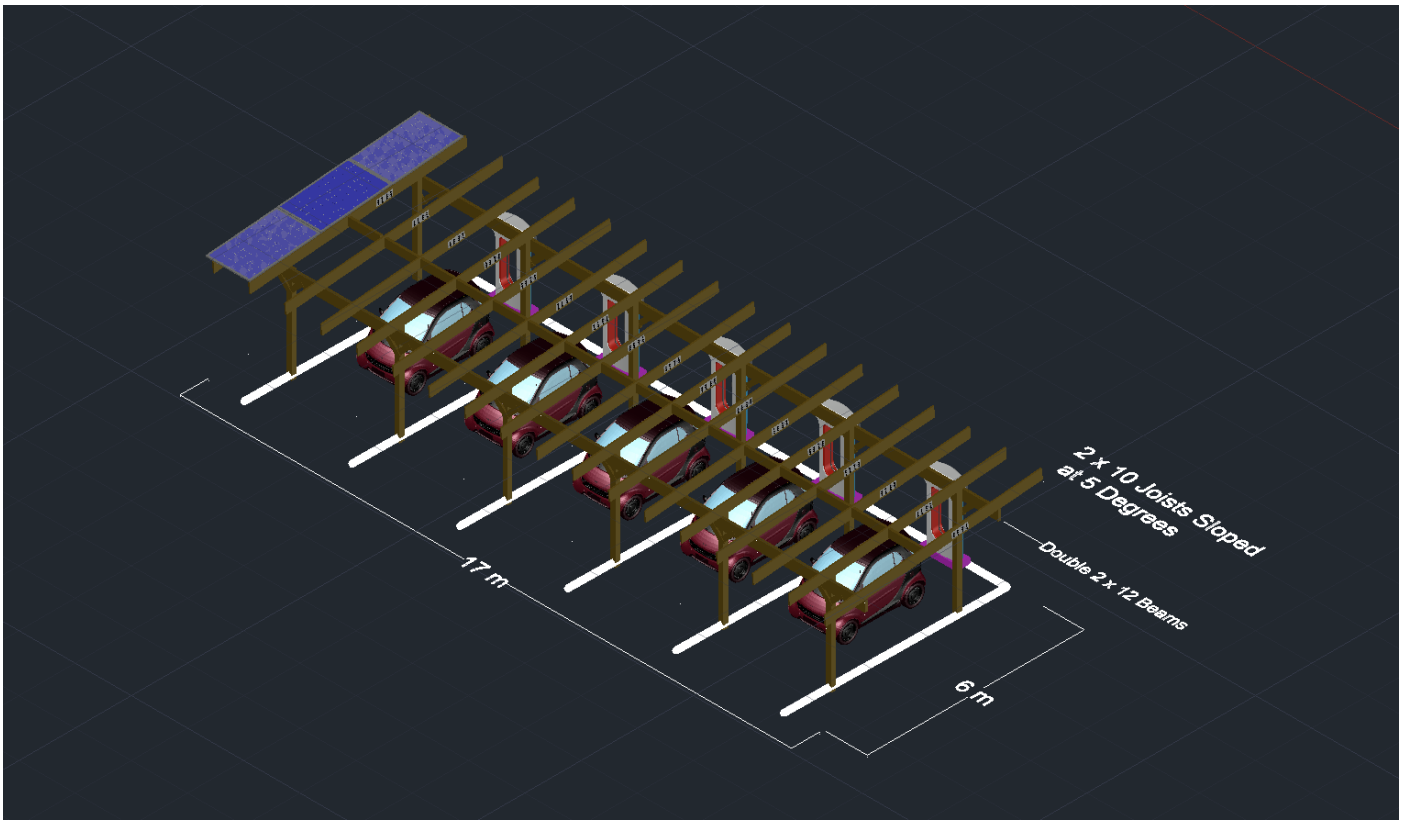

Figure 6. Finished Single-Span System.

3.2 Double Spanning System

3.2.1 Double Spanning System Bill of Materials

The BOM of the two-span system is shown in Table 3 in Canadian dollars sourced from Copp's Build-All, London, and Metal Supermarkets, London.

Preprints (www.preprints.org) | NOT PEER-REVIEWED | Posted: 13 September 2022 doi:10.20944/preprints202209.0174.v1

Table 3. Two-Span System Bill of Materials.

Member Name	Piece[1]	Cost per Piece[2]	Quantity	Cost
Joists	2 x 10 x 14	$53.99	21	$1,133.79
	2 x 10 x 12	$46.28	11	$509.08
T6 6061 Aluminum Beam	4 x 8 x 0.270 x 20 m	$7120	2	$14,240.00
Joist Splice Tie Plate	3 x 5 Mending Plate	$2.25	24	$54.00
Beam Splice Tie Plate	3 x 7 Mending Plate	$2.79	12	$33.48
Lateral Bracing	2 x 10 x 14	$53.99	5	$269.95
Joist to Beam Ties	H1 Hurricane Ties	$2.19	34	$74.46
Posts	6 x 6 x 16	$88.74	8	$709.92
Post Lateral Diagonals	4 x 4 x 14	$33.89	2	$67.78
Screws	2-1/2" Deck Screws (1175/pail)	$38.99	1	$38.99
D10 Nails	1-1/2" Joist Hanger Nails	$4.65	5	$23.25
Self-Tapping Screws	#10 x 2" 100 Pack	1	$15.09	$15.09
Module to Joist Connection	¼" x 2-1/2" Carriage Bolt, Nut, and Washer	$1.01	204	$206.04
			Total Cost with No Concrete	$17,375.83
Concrete for Posts	30 MPa Quikrete concrete	$5.55	100 bags	$555.00
			Total Cost:	$17,930.83

[1] All lumber is to be pressure treated, and all hardware is to be hot dipped galvanized.
[2] All costs are in Canadian Dollars as of December 13, 2021, before tax.
[3] 1 piece to be cut to serve as 2 front posts.
[4] Cost per connection (1 bolt, 1 nut, 1 washer).

3.2.2 Double Span System Assembly Instructions

6 x 6 posts are installed in the same manner as the single span system, but now are spaced 2 parking spots apart. 4 x 8 x 0.270 T1 6061 aluminum beams are connected on top of the posts. Connections are secured with 4 self-tapping screws installed from the bottom flange, down to the bottom of the wood post. Aluminum beams may be available in full lengths, but splice joints can be made to satisfy supply and transportation constraints. Joists and braces are connected in the same manner as the single span system. The final system is shown in Figure 7.

Preprints (www.preprints.org) | NOT PEER-REVIEWED | Posted: 13 September 2022 doi:10.20944/preprints202209.0174.v1

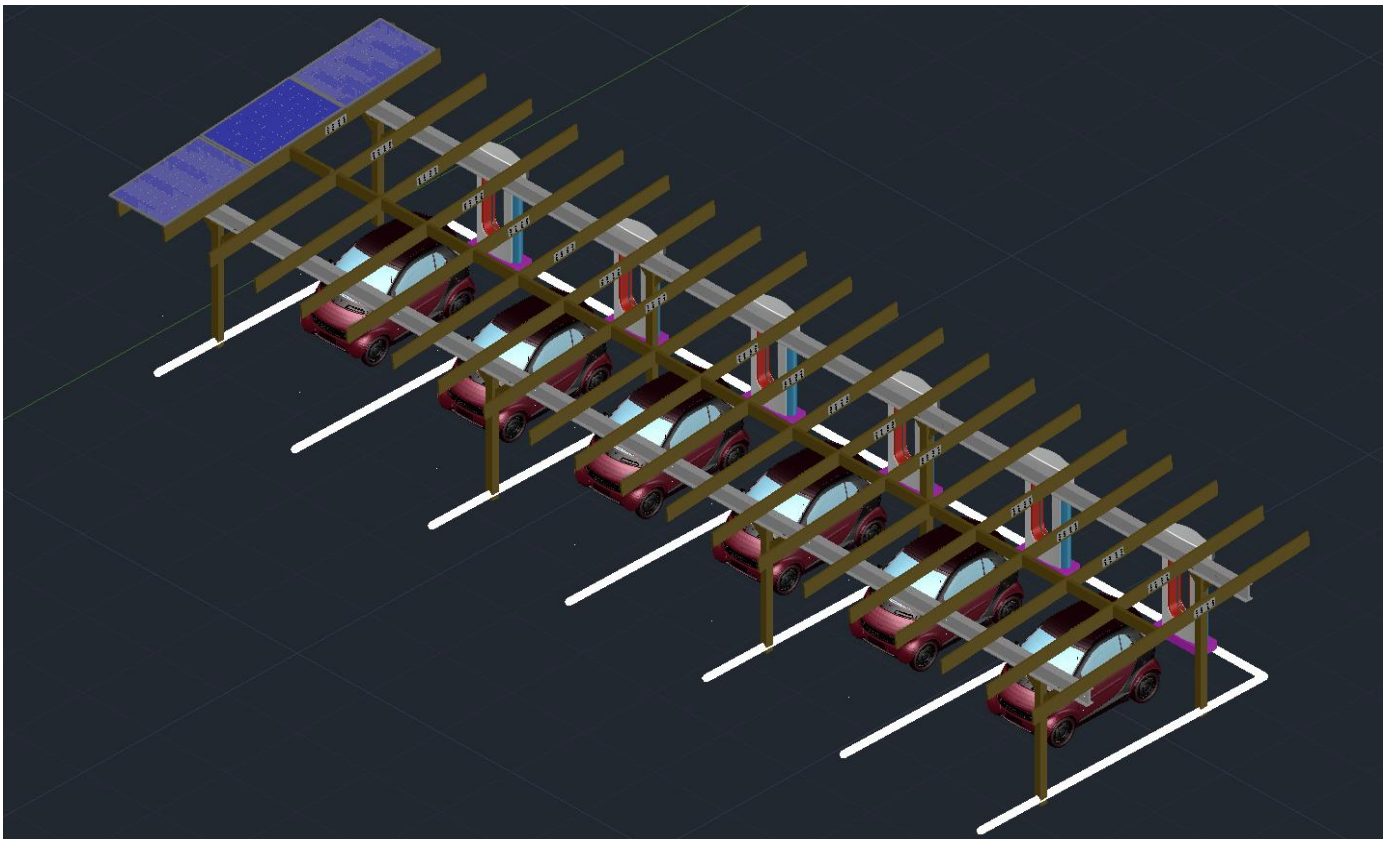

Figure 7. Completed Double Span System, constructed in the same way as the Single Span System, but with aluminum I beams being installed on top of the 6 x 6 posts with self-tapping screws.

Preprints (www.preprints.org) | NOT PEER-REVIEWED | Posted: 13 September 2022 doi:10.20944/preprints202209.0174.v1

3.3 Cantilevered System

3.3.1 Cantilevered System Bill of Materials

The BOM of the cantilevered system, which is appropriate for on the street parking, is shown in Table 4 in Canadian dollars sourced from Copp's Build-All, London, and Metal Supermarkets, London.

Table 4. Cantilever System List of Materials

Member Name	Piece[1]	Cost per Piece[2]	Quantity	Cost
Joists	2 x 10 x 16	$61.71	30	$1,851.30
	2 x 10 x 10	$38.57	10	$385.70
T6 6061 Aluminum Beam	4 x 8 x 0.270 x 4 m	$1424	11	$15,664.00
Joist Splice Tie Plate	3 x 5 Mending Plate	$2.25	30	$67.50
Lateral Bracing	2 x 10 x 14	$53.99	10	$539.90
Joist to Beam Ties	H1 Hurricane Ties	$2.19	68	$148.92
Posts	8 x 8 x 16	$214.88	11	$2,363.68
Post Lateral Diagonals	6 x 6 x 16	$88.74	4	$354.96
Screws	2-1/2" Deck Screws (1175/pail)	$38.99	2	$77.98
D10 Nails	1-1/2" Joist Hanger Nails	$4.65	10	$46.50
Self-Tapping Screws	#10 x 2" 100 Pack	$15.09	2	$30.18
Aircraft Cable	5/16" 7x19 Galvanized	$6.67	44	$293.48
Module to Joist Connection	¼" x 2-1/2" Carriage Bolt, Nut, and Washer	$1.01[3]	256	$258.56
			Total Cost with No Concrete	$22,082.66
Concrete for Posts	30 MPa Quikrete concrete	$5.55	102 bags	$1,037.85
			Total Cost:	$23,120.51

[1] All lumber is to be pressure treated, and all hardware is to be hot dipped galvanized.
[2] All costs are in Canadian Dollars as of December 13, 2021, before tax.
[3] Cost per connection (1 bolt, 1 nut, 1 washer).

3.3.2 Cantilevered System Assembly Instructions

For the cantilevered system, 8 x 8 posts are spaced 3 m apart at each parking spaces corners, being 3.6 m in length as shown in Figure 8.

Preprints (www.preprints.org) | NOT PEER-REVIEWED | Posted: 13 September 2022 doi:10.20944/preprints202209.0174.v1

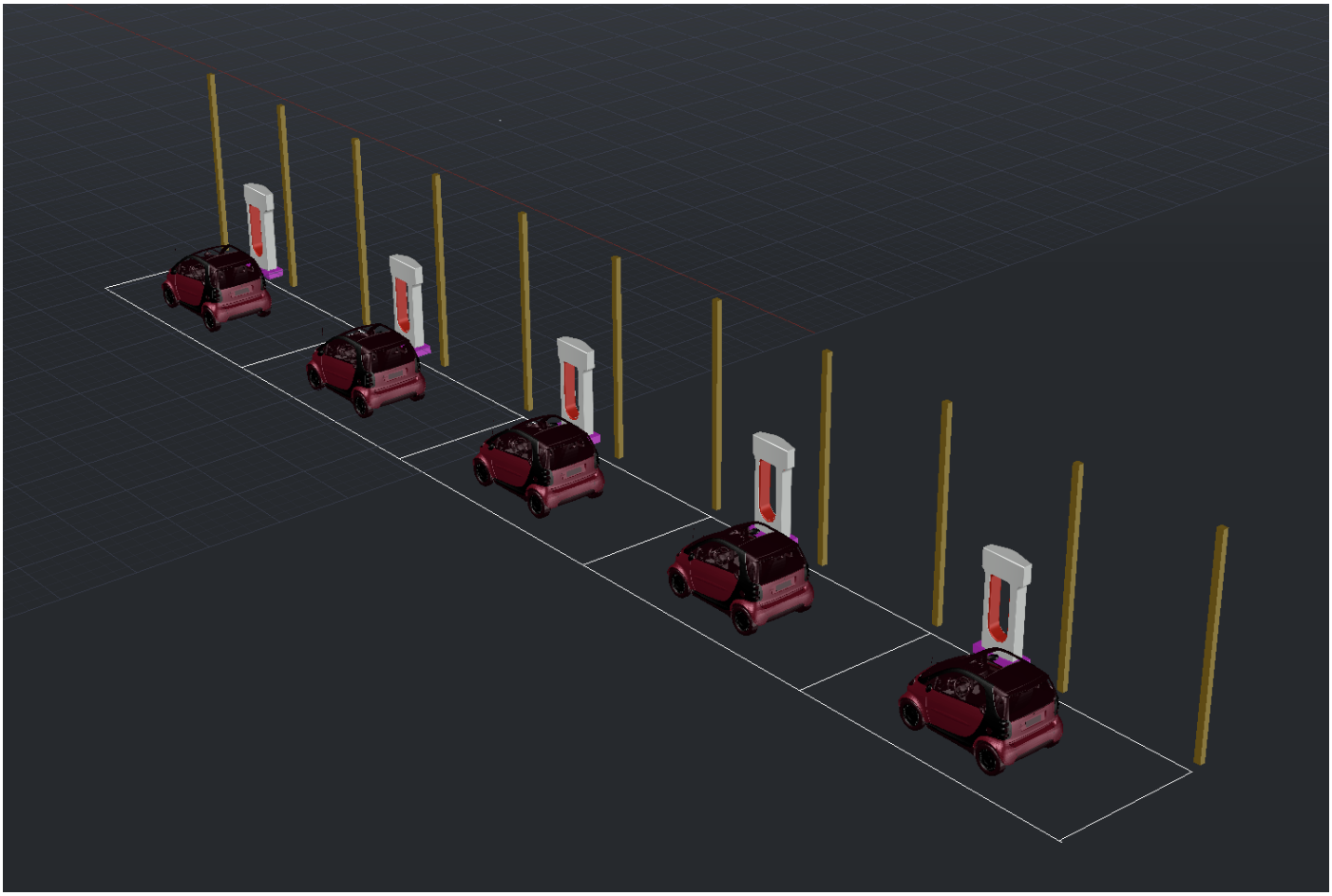

Figure 8. Post arrangement for the Cantilevered System.

Then, 4 m long 4 x 8 x 0.270 aluminum beams are installed at 5 degrees on top of each post with self-tapping screws in the same manner was the double spanning system as outlined in Figure 9. Then, ¼" 7 x 19 strand galvanized aircraft cable is installed on the back of the aluminum beam, directly into the ground to prevent tipping. 4 x 4s can be screwed onto the 8 x 8 posts to serve as diagonal bracing to support each cantilevered beam. Connect these 4 x 4 s with self-tapping screws.

Preprints (www.preprints.org) | NOT PEER-REVIEWED | Posted: 13 September 2022 doi:10.20944/preprints202209.0174.v1

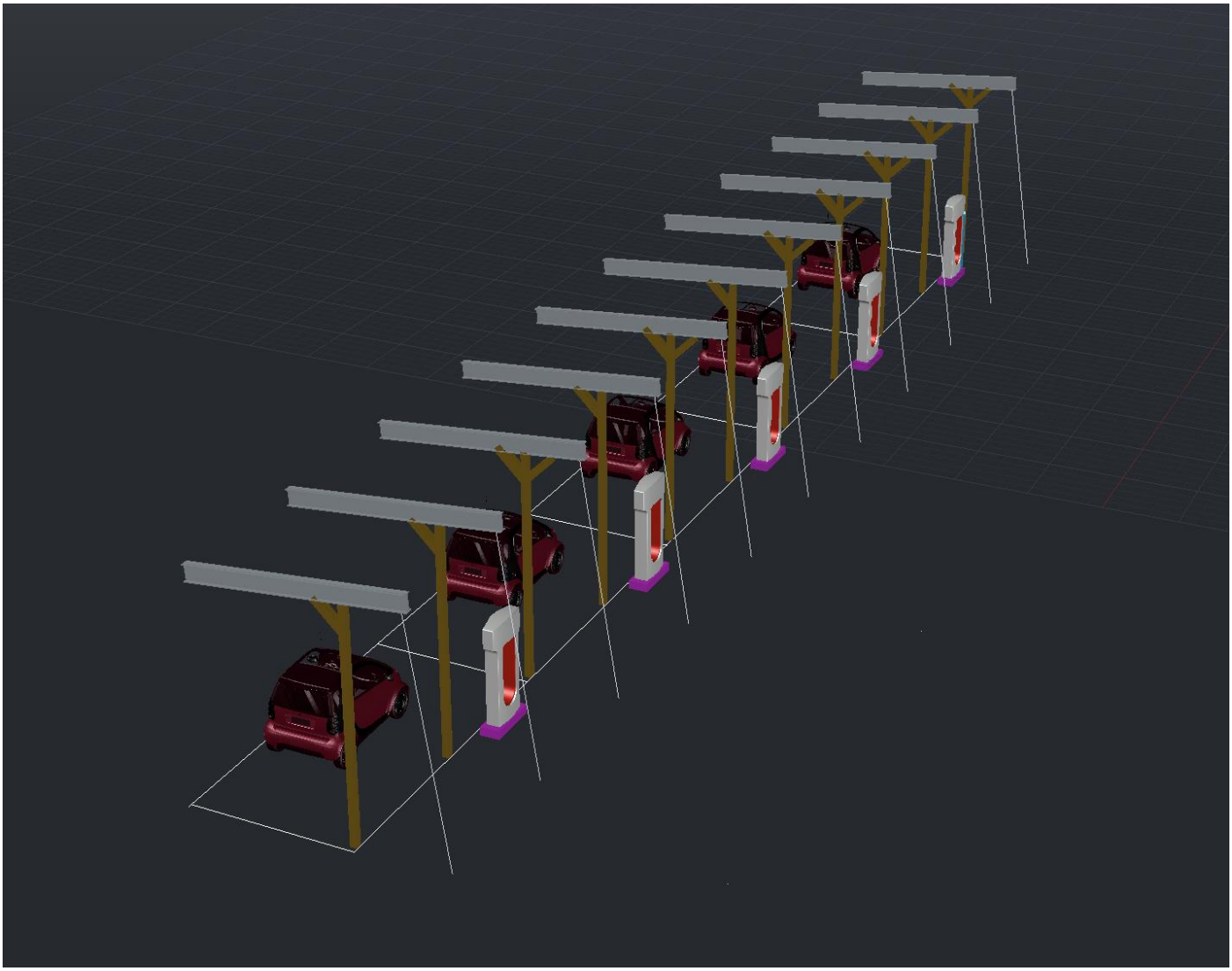

Figure 9. Aluminum Beams installed onto 8 x 8 posts, angled at 5 degrees, and supported with ¼" 7 x 19 strand galvanized aircraft cable and diagonal bracing.

2 x 10 joists are then installed horizontally across the aluminum beams. Splice joints are to be made at 20% of the span length away from each beam. Use H1 hurricane ties with self-tapping screws to connect the ties to the beam, and joist hanger nails to connect the ties to the wood. 1 m long lateral braces are installed between each beam. The final cantilevered system is shown in Figure 10. The cables would be anchored in the road verge, which is normally a strip of grass located between a roadway (carriageway) and a sidewalk (pavement). This curbside system provides the potential to have PV canopies on the sides of streets to charge EVs that only have street parking. Substantial future work is needed to investigate the regulatory and legal ramifications of such systems as the road verge and street are normally owned by the municipality.

Preprints (www.preprints.org) | NOT PEER-REVIEWED | Posted: 13 September 2022 doi:10.20944/preprints202209.0174.v1

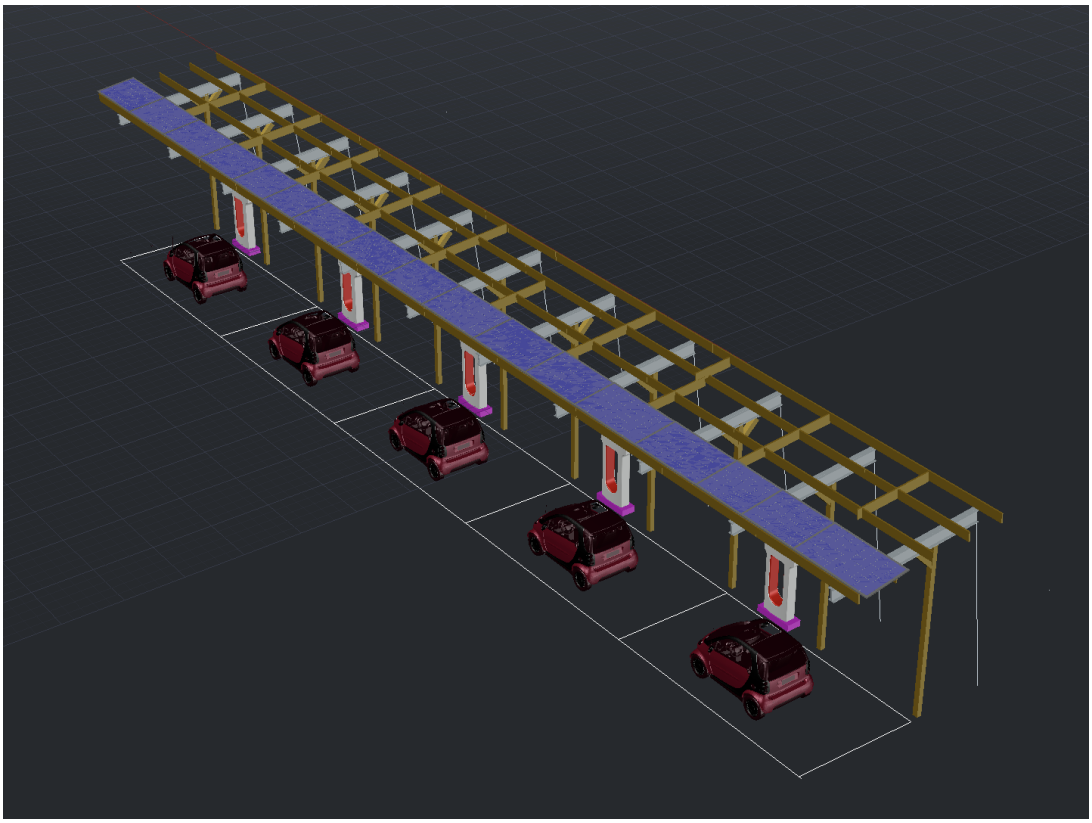

Figure 10. Final Cantilevered System

3.4. Economic Analysis

3.4.1 System Cost Comparison

The cost per W for each system has been summarized in Table 5. It should be noted that the double span system can only be built in multiples of 2, and so a 6-spot system is built instead of a 5-span system. Nevertheless, the systems are broken down into cost per W, making this a fair cost comparison between the systems.

Table 5. Cost per W for each system in $CAD.

System	Size	Cost	Cost per W
5 Spot Single Span	3 x 17 @ 410 W = 20.91 kW	$4,648.49	$0.2223
6 Spot Double Span[1]	3 x 20 @ 410 W = 24.60 kW	$17,930.83	$0.7289
5 Spot Cantilevered	16 x 4 @ 410 W = 26.24 kW	$23,120.51	$0.8811

[1] This system spans in multiples of 2, thus a 6-parking spot system is used for this analysis.

Preprints (www.preprints.org) | NOT PEER-REVIEWED | Posted: 13 September 2022 doi:10.20944/preprints202209.0174.v1

3.4.2 System Size Cost Sensitivity

The total cost and cost per W for varying system sizes is shown in Table 6.

Table 6. Cost per W for each system in $CAD.

Spans	Parking spots	Size	Cost	Cost per W
Single	2 Spot	3 x 8 @ 410 W = 9.84 kW	$2,409.16	$0.2448
	10 Spot	3 x 32 @ 410 W = 39.36 kW	$8,696.37	$0.2209
	20 Spot	3 x 62 @ 410 W = 76.26 kW	$16,744.87	$0.2196
Double	2 Spot	3 x 8 @ 410 W = 9.84 kW	$7,198.93	$0.7316
	10 Spot	3 x 32 @ 410 W = 39.36 kW	$27,664.54	$0.7029
	20 Spot	3 x 62 @ 410 W = 76.26 kW	$53,515.80	$0.7018
Cantilevered	2 Spot	7 x 4 @ 410 W = 11.48 kW	$10,263.87	$0.8941
	10 Spot	31 x 4 @ 410 W = 50.84 kW	$43247.39	$0.8507
	20 Spot	61 x 4 @ 410 W = 100.04 kW	$81,785.03	$0.8175

[1] This system spans in multiples of 2, thus a 6-parking spot system is used for this analysis

3.4.3 Material Cost Sensitivity Analysis

The price of lumber has been extremely volatile as shown in Figure 11. In the last decade, the cost of lumber reached record highs in the COVID-19 pandemic, and as low as 41% and as high as 281% of the current price [66]. This means that the single-span wood system would effectively range from $0.62 CAD per W to $0.09 CAD per W to install. Thus, using wood as a cost-effective alternative to aluminum and steel is highly dependent on the timing of purchase.

Figure 11. Lumber Prices in USD in the last decade.

Additionally, the cost of aluminum has also been volatile. Prices have been as low as 60%, and as high as 160% of the current price [67] as shown in Figure 12.

Preprints (www.preprints.org) | NOT PEER-REVIEWED | Posted: 13 September 2022 doi:10.20944/preprints202209.0174.v1

Figure 12. Aluminum Prices in USD in the last decade.

While there are many other factors such as labor and transportation that impact the cost of the final product, it is valid to assume that changes in the commodity price of these materials directly translates to changes in the final retail cost. The peaks and troughs between wood and aluminum prices occur nearly at the same time, specifically the largest spike in early 2022, and the lowest point in early 2020. A summary of the range of price in these systems is outlined in Table 7.

Table 7. System cost sensitivity based on material commodity prices, in $CAD.

System	Current Cost per W	Low Cost per W[1]	High Cost per W[2]
5 Spot Single Span	$0.2223	$0.0911	$0.5336
6 Spot Double Span	$0.7289	$0.4027	$1.2451
5 Spot Cantilevered	$0.8811	$0.4745	$1.6374

[1] Assuming a 41% increase in wood, and 60% increase in aluminum.
[2] Assuming a 240% increase in wood, and 160% increase in aluminum.

3.4.4 Location Cost Sensitivity Analysis

The cost of these systems is highly based on the availability of the structural materials in that location. Table 8 of Vandewetering et al. outlines how pressure treated lumber is noticeably higher in other continents than in North America, where a standard 2 x 4 in Togo is about 2.5 times the cost of one in Canada [46], and thus a wooden system in this region would not be economically practical to build. The cost of aluminum varies based on the tariffs in place on importing, and local availability. China, India, and Canada are examples of countries with the largest aluminum production [68], making the I beams extremely affordable in these major countries. Locations such as the Bahamas and Bermuda, however, have tariffs of up to 40.2% on raw aluminum [69], thus making the two-span and cantilevered system in these regions relatively less affordable. These systems are especially cost efficient in North America, but future work can be done to build similar systems with accessible materials such as concrete and recycled plastic.

3.5. Energy Analysis Results

To analyze the load match between the PV system and EV charging station, the energy production of the PV system and the load demand of the EV are plotted for different types of charging sites and different charging power level as per the North American Standards. The results are shown for the day with the maximum energy production and the day with the lowest energy production in Figure 9 and Figure 10, respectively. The "Home Type 1" in Figure 9 and Figure 10 indicates an EV charging station located at a

Preprints (www.preprints.org) | NOT PEER-REVIEWED | Posted: 13 September 2022 doi:10.20944/preprints202209.0174.v1

users' home where the users return home from work during the middle of the day and goes back to work in the afternoon. This would be for example at an apartment complex. On the other hand, in the "Home Type 2" scenario, the users only return home after 4 pm [62]. In all of these cases the charger is used for multiple EVs.

Figure 13 shows that for a level 1 type charging station, the PV system will produce enough energy to cover the needs of the station running 24 hours/day using the load profile proposed by Zhang et al. [62]. In the case of the type 1 home charging station, the peak demand of the EV load matches the peak production of the PV. For the type 2 charger station, however, the peak EV demand is skewed to the right of the peak energy production of the PV. Therefore, for a type 2 home EV charging station, the system will import part of its energy from the grid if being used to charge multiple EVs. Level 2 and level 3 charging stations have the same load-matching profiles as level 1. The main difference is that in the level 3 charging profiles, a single carport PV system does not possess the instantaneous power to match to high-powered charging station. Therefore, if a level 3 charging station is considered for the proposed carport, more than one carport is needed, and a more sophisticated charging scheme would need to be investigated in future studies to share EV loads between multiple carports. Figure 14 shows the match between the PV system and the EV charging stations for a wintery day where there is minimum energy generation. Expectedly, the PV system is not generating sufficient energy to provide the needs of the charging station, and most of the charging energy will be drawn from the grid.

Preprints (www.preprints.org) | NOT PEER-REVIEWED | Posted: 13 September 2022 doi:10.20944/preprints202209.0174.v1

	Home Type 1	Home Type 2	Workplace
Level 1 (Max Power = 1.4 kW)	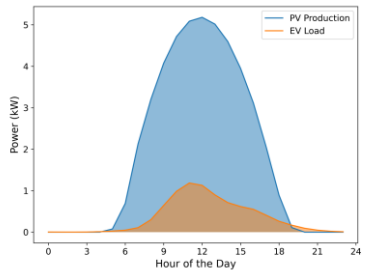	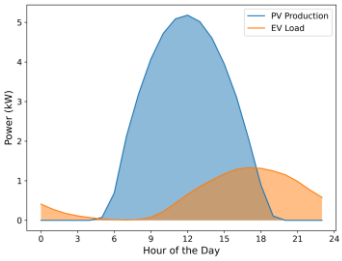	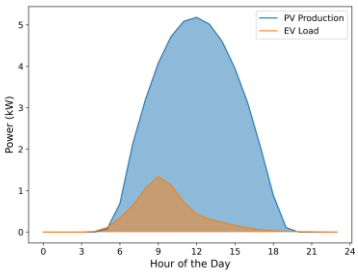
Level 2 (Max Power = 8 kW)	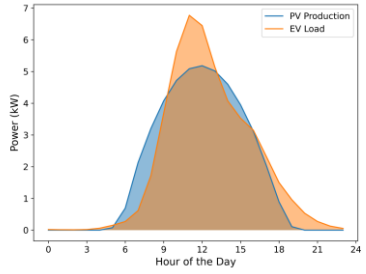	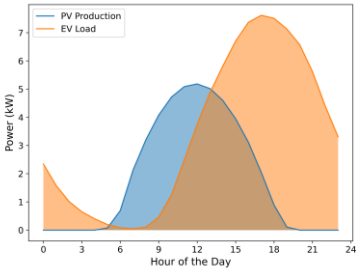	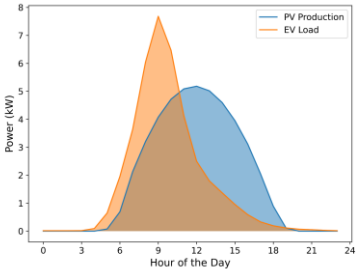
Level 3 (Max Power = 50 kW)	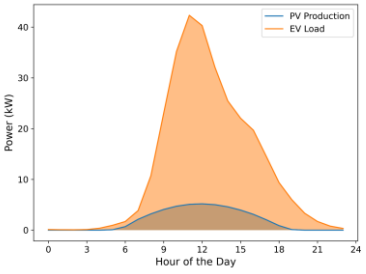	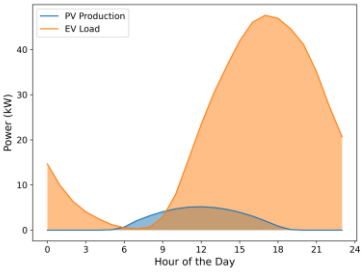	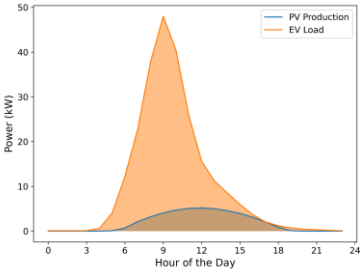
Level 3 (Max Power = 100kW)	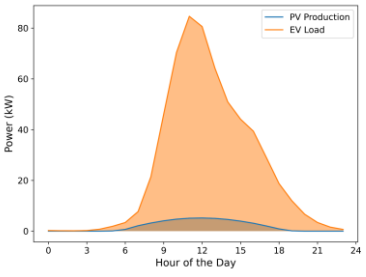	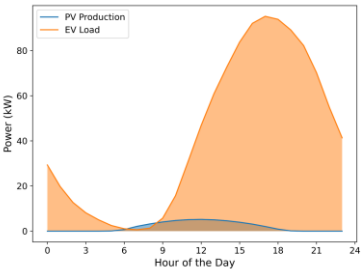	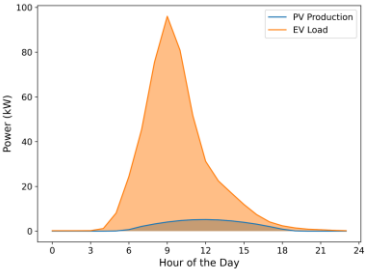

Figure 13. Load matching results (kW) between the PV system and EV charging stations supplying multiple EVs, using the load profiles proposed by Zhang et al. [62], for the day with maximum energy production (June 26) in London Ontario. The three levels of EV charging stations in the North American EV standards are used. The load matching is plotted in different charging locations. In **Home Type 1**, the EV users come back home at noon.

Preprints (www.preprints.org) | NOT PEER-REVIEWED | Posted: 13 September 2022 doi:10.20944/preprints202209.0174.v1

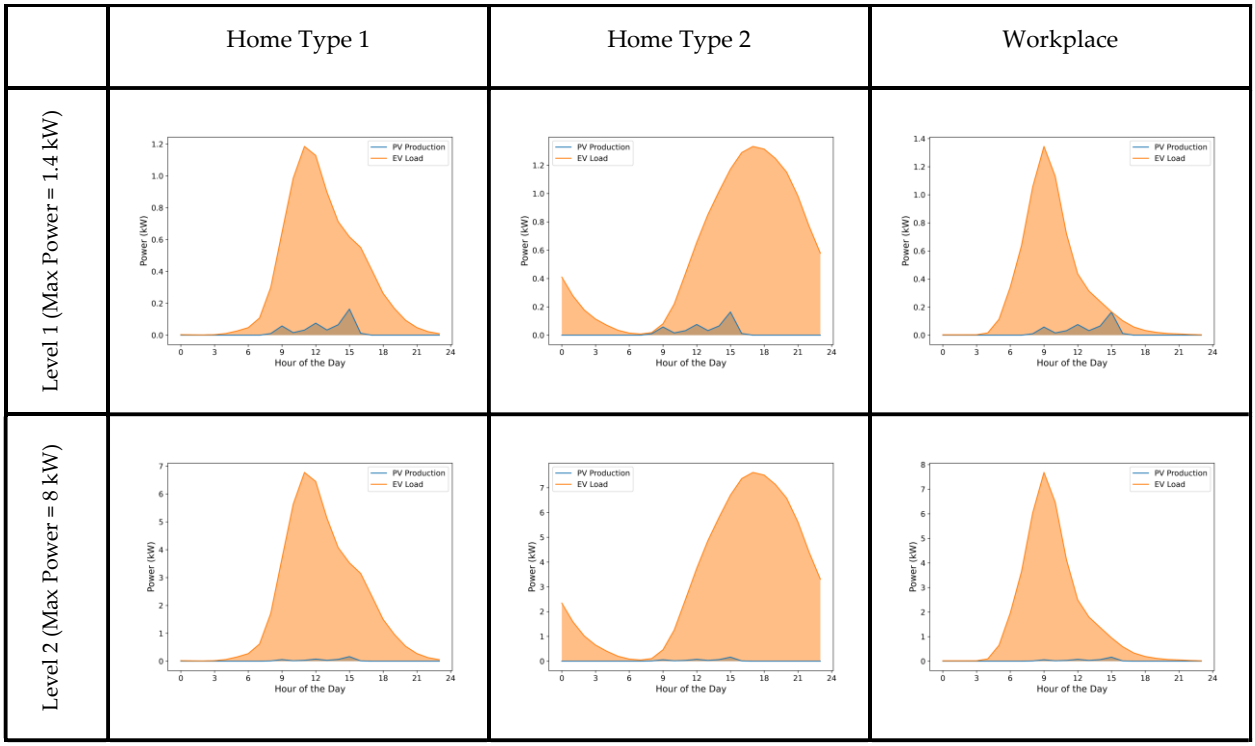

Figure 14. Load matching results (kW) between the PV system and EV charging stations supplying multiple EVs, using the load profiles proposed by Zhang et al. [62], for the day with the minimum energy production (December 24) in London Ontario. The first two levels of EV charging stations in the North American EV standards are used. The load matching is plotted in different charging locations. In **Home Type 1**, the EV users come back home at noon.

Figure 15 shows the cumulative monthly energy generated by the PV and the monthly energy demand for each power charging station level in the case of a type 1 home. For the level 1 charging station (1.4 kW) the PV system produces more energy than required by the charging station and a surplus of 4.532 MWh is injected into the grid during the first year of operation. For each of the subsequent charging power levels, however, the PV energy does not cover the charging station needs during the year. Specifically, the charging station will draw 9.03 MWh, 95.35 MWh, and 191.12 MWh from the grid in the case of level 2 (8 kW), level 3 (50kW), and level 3 (100kW) charging systems, respectively. This shows that the proposed carport design is suitable for a level 1 charging system if multiple EVs with different features are charged throughout the day.

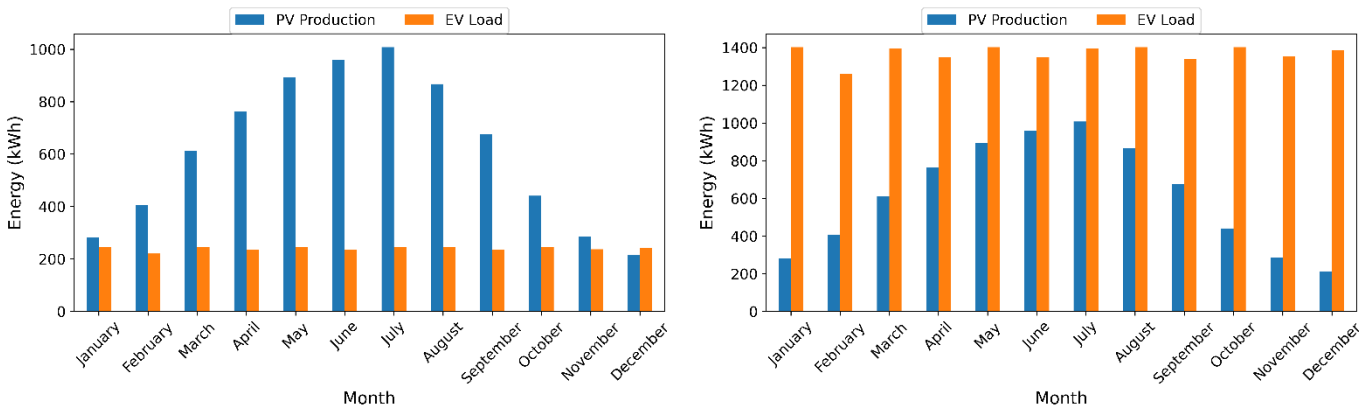

a) b)

Preprints (www.preprints.org) | NOT PEER-REVIEWED | Posted: 13 September 2022 doi:10.20944/preprints202209.0174.v1

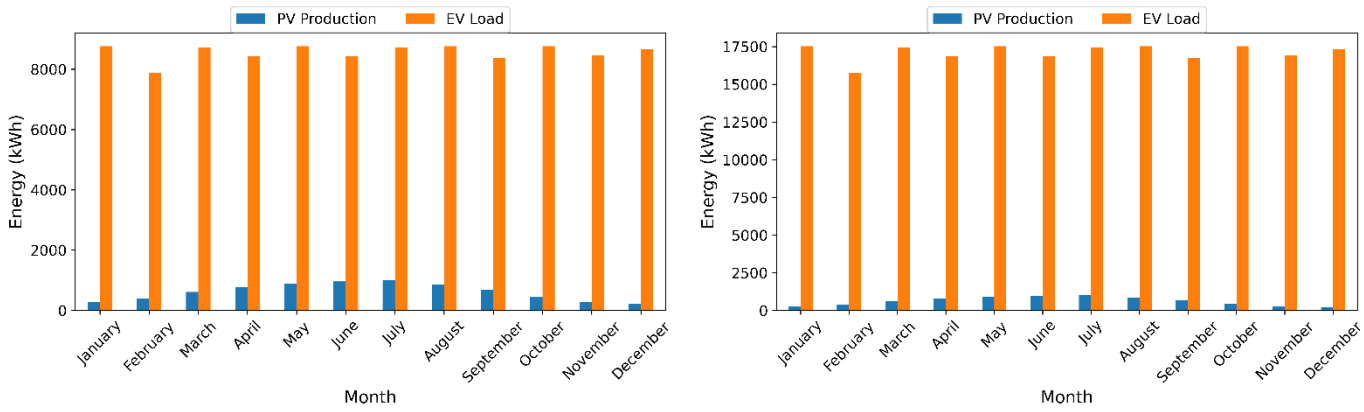

Figure 15. Monthly cumulative energy production (kWh) of the PV system and the charging load for the three levels of charging stations in the case of a Type 1 Home (EV user returns home at noon). (a) Level 1 charging station 1.4 kW. (b) Level 2 charging station 8 kW. (c) Level 3 charging station 50 kW. (d) Level 3 charging station 100 kW.

The energy balance shown in Figure 15 is calculated annually for all types of systems (type 1 home, type 2 home, workplace) and all charging levels (level 1 to level 3). The calculation is performed for two locations, London ON, and Los Angeles California. The results show that in each case, the level 1 type charger (1.4 kW) is suitable for the operation regardless of the charging site. For a level 1 charger, the PV system has a net positive balance. For the other power level (type 2 and type 3), the system has a net negative balance, as more energy is drawn from the grid assuming they are operating full time using the charging load profiles proposed by Zhang et al. [62]. The location impact is shown by Los Angeles having a better energy balance compared to London ON. This is directly related to the solar irradiation in each location. But this location impact is not significant when deciding which charging power level to use with the proposed solar PV carport for multiple EVs.

Preprints (www.preprints.org) | NOT PEER-REVIEWED | Posted: 13 September 2022 doi:10.20944/preprints202209.0174.v1

Table 8. Comparison of the annual energy balance (MWh) of a single PV carport and a charging station (charging multiple EVs) between London ON, and Los Angeles. The comparison accounts for different charger power levels and different charging sites. Positive values represent energy injected into the grid by the PV system and negative values are energy drawn from the grid.

Charger Power Level	Home Type 1 (MWh)		Home Type 2 (MWh)		Workplace (MWh)	
	London ON	Los Angeles	London ON	Los Angeles	London ON	Los Angeles
Level 1 Charger (1.4 kW)	4.5	7.1	2.2	4.7	4.9	7.4
Level 2 Charger (8 kW)	-9.0	-6.5	-22.4	-19.9	-7.0	-4.5
Level 3 Charger (50 kW)	-95.4	-92.8	-179.1	-176.5	-82.9	-80.4
Level 3 Charger (100kW)	-198.1	-195.6	-365.5	-362.9	-173.3	-170.7

In the specific case where the proposed PV carport is used for a single individual EV in a net-metered system, Figure 16 shows the PV system annual energy production will cover the average yearly energy needs of the EV. In the case of London Ontario, which results are displayed on Figure 16, the average annual energy demand of a single EV varies between 1,744 kWh and 4,720 kWh depending on the make and the model of the EV. On the other hand, the PV carport generates 7,409 kWh annually. This means the proposed PV carport, when connected to a net metered grid, can produce far more than sufficient energy to charge one EV available on the market currently (and depending on the driving behavior and selection of EVs could charge more than one or provide some power for the home). It should be noted, however, that this observation will fluctuate with the driving pattern of the vehicle owner. In the future, if the progression in technology increases EV capacities above 463 Wh/km, then a bigger carport would be needed for charging a single EV. Even so, PV modules energy density and efficiencies are increasing as well and would be able to keep up with the increase in EV efficiencies.

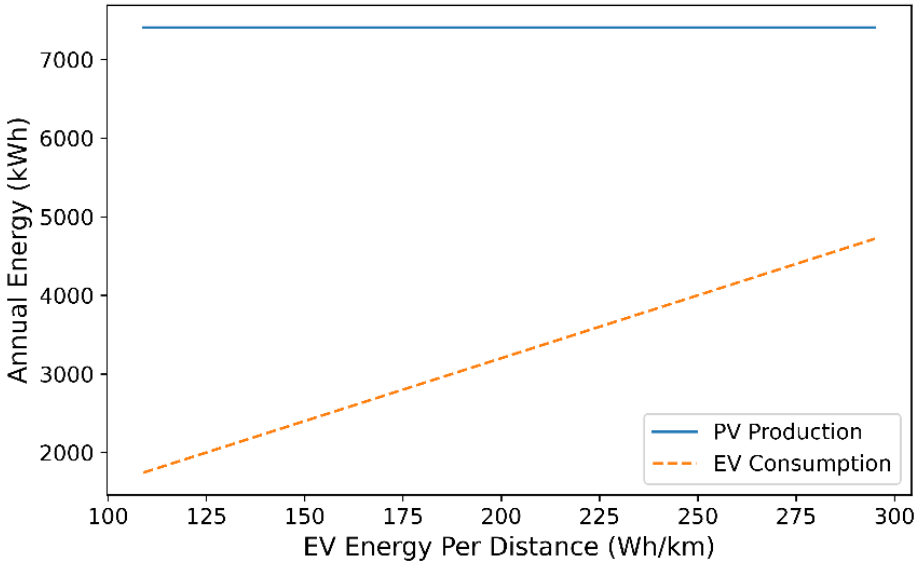

Figure 15. Comparison of the annual energy production of a single PV carport using 20.51 % efficient PV (reference efficiency) to the average annual energy needs of a single EV in London Ontario. The value of current EVs on the market are used for the EV energy per distance.

4. Discussion

4.1 Benefits

Economically, these systems have a significant advantage over conventional steel and aluminum carports proposed today. Considering that typical carport systems designed for PV has a cost range of $1.30-$1.50 per W [44,45,70], the single-span system has cost

Preprints (www.preprints.org) | NOT PEER-REVIEWED | Posted: 13 September 2022 doi:10.20944/preprints202209.0174.v1

savings of 82%-85%, the double-span system has cost savings of 43%-50%, and the cantilevered system has savings of 31%-40%.

Compared to wooden ground mounted systems, the carport canopies are less cost and energy efficient, considering ground mounted systems can be as low as $0.32 CAD per W, and are even installed to the optimal tilt angle based on geographical location to provide greater energy yield [46]. Future work can be completed to design carport systems at optimal tilt angles, or even allow for varying tilt angles to minimize this difference in efficiency. Nevertheless, the 5-degree carport system offers a sleek and practical design that clears at least 3 m from the ground, thus the modules are not consuming critical land area.

Compared to conventional metal ground mounted PV racks, small scale residential racks range from $0.57 CAD per W [71] to $1.27 CAD per W [72]. Commercial systems cost $0.71 CAD per W [73]. Thus, users of the single-span wooden system can also see significant cost savings with the installation of a carport system.

Since these systems are ideally DIY builds, the labor costs are excluded. Future work is needed to quantify construction times of these systems to provide labour costs. In previous projects, labor costs have been approximately 20% of the material costs [45], which effectively means the approximate labor costs for the single-span, double-span, and cantilevered systems are $929.69, $3586.17, and $4624.10 respectively.

From comparing the sensitivity results in Table 6 to the base results in Table 5, it is clear that larger scaled systems are more cost effective than small scale systems. For example, in the single span system, cost savings are over 10% per W when a 20-stall system is built over a 2-stall system. This is because outside posts and joists are structurally and financially inefficient because they carry half the load of the inside posts, so when a system is scaled up, the percentage of inefficient outside members decreases, and thus, cost efficiency increases. These efficiencies only include the base material costs. It should be pointed out that as system sizes increase, there may also be opportunities to take advantage of bulk pricing for large systems or to arrange for large purchases and offer kit sales for many small individual systems.

Canopies have the benefit of shading the vehicle, which reduces the users need for air conditioning, and can protect children and pets from heat-related deaths being trapped in vehicles exposed to direct sunlight even in low-outdoor temperatures [74]. Additionally, the coverage of the carport prevents users from needing to clear off ice and snow from their vehicle in the winter months. These secondary benefits of the carport design provide users with additional convenience, comfort, and safety beyond charging the vehicle.

The PV canopies are also likely to reduce the urban heat island effect caused by dark paved surfaces [75]. Golden et al. [76] found that PV provide an even greater thermal reduction than urban forests.

Moreover, the cantilevered system has the benefit of being reoriented to cover vehicles in a parking lot of the same orientation as the other two systems as shown in Figure 16. This system orientation is ideal for parking spots on the end of a lot since the steel cable gets in the way of interior parking spots. Additionally, it should be noted that this system can only shade half of the parking spot and half the energy yield when assembled in this orientation, so it is recommended to select one of the other systems for this application, unless posts cannot be installed directly into the lot.

Preprints (www.preprints.org) | NOT PEER-REVIEWED | Posted: 13 September 2022 doi:10.20944/preprints202209.0174.v1

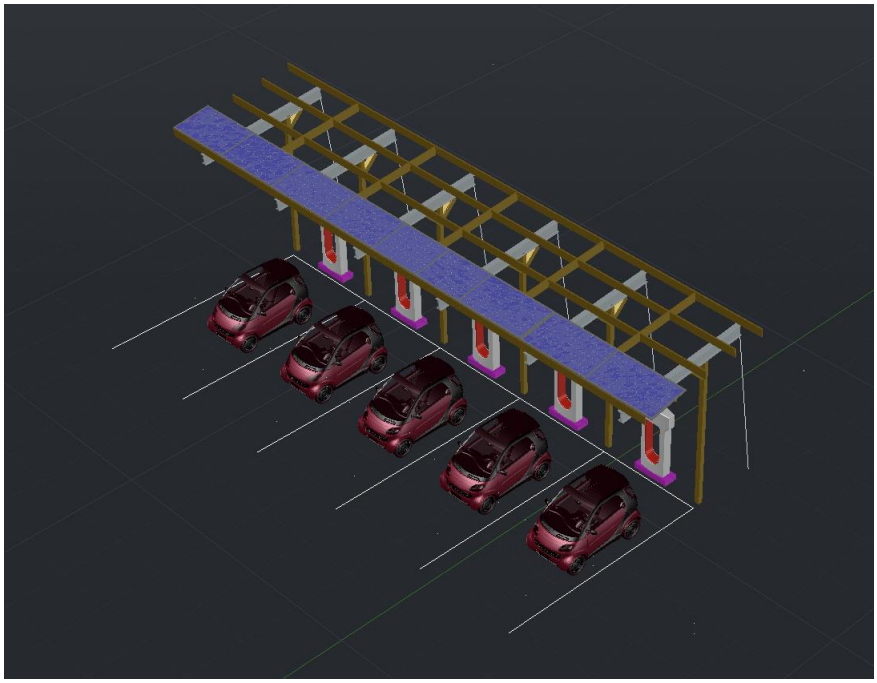

Figure 16. Cantilevered system reoriented for outsides of parking lots.

4.2 Limitations and Future Work

There may be difficulty in installing the footings from system 1 and 2 into existing parking lots. Users will have to rent a jackhammer to cut through the asphalt, then auger through a dense gravel layer before native soil is exposed. This results in higher labor and equipment costs.

The double spanning system is scaled in multiples of 2; it is not ideally designed for an odd number of parking spots. A user can decide to build this system for an odd number of spots, as in they build the last span to only cover one spot, but this is an inefficient use of the structural capabilities of the aluminum beams, and thus the user can expect a higher cost per W for their build.

With the promotion of open source carport canopies, these designs demand that future work is to be done to develop an open source EV charging station, and thus, a completely open source PV-EV charging system can be developed to further drive the costs of these systems down, making them more accessible to the general public, and even home owners. There has already been substantial efforts made on this front in the OpenEVSE project [77] where a 48A/40A model is available for USD$600 and kit can be purchased for USD$300 [77].

If a single car system for home DIY design wants to be made, the one copy of the single-span system can easily be made as shown in Figure 17. The single car system allows for a 3 x 5 array to be assembled, allowing for 6 kW of PV power to charge the vehicle. This racking system costs approximately $1,565.00 CAD, which corresponds to $0.26 per W. The average Canadian cost of modules is $0.91 per W [78–82]. Thus, a single car system, including the model, kit, and PV modules could be fabricated in Canada for $8193.83 ($1.36 per W) and in the US for $6,309.25 or $1.05 per W.

Preprints (www.preprints.org) | NOT PEER-REVIEWED | Posted: 13 September 2022 doi:10.20944/preprints202209.0174.v1

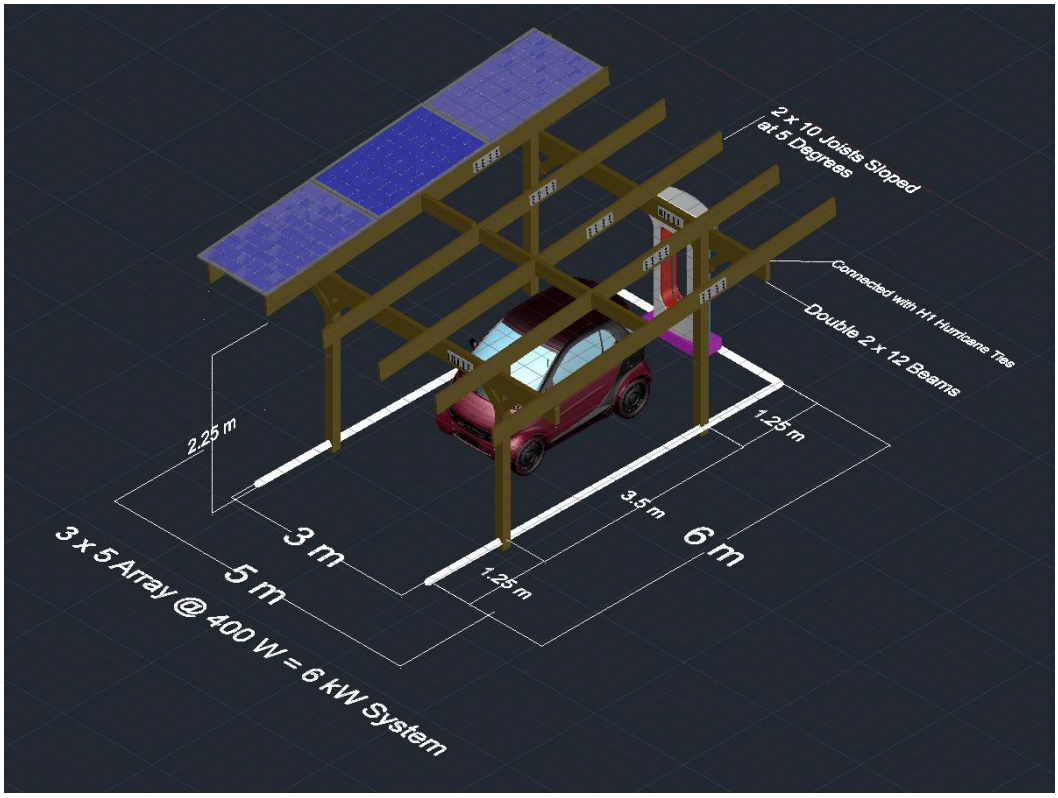

Figure 17. Single Car System for home DIY designs.

Thus, an economical open source carport PV canopy and EV charger could be constructed using the designs in this study and those from OpenEVSE. Future work is necessary to further investigate the full economics of the system including the potential to integrate storage and thus use the PV+EV charger as an off-grid system to avoid any interconnection friction and/or anti-distributed solar policies developed by utilities to maintain monopoly profits [83–85]. The results of the energy modeling for different EV charger types provides a baseline of data for such analysis, but future work would need to investigate different rate structures for utilities that do not have full annual net metering rate structures. For a completely open source system, which minimizes costs, further work is needed in open source charge control and inverters as well as open source PV modules.

5. Conclusions

This study has provided the full BOM, designs and instructions for fabricating three low-cost PV-EV canopy systems as well as economic and energy simulations and analysis. The results clearly showed that the use of wood for PV canopies can substantially reduce the capital costs of the systems making them potentially attractive investments from the scale of a single carport in a single-family home to covering a large business or institution parking lots. The single-span system has cost savings of 82%-85%, the double-span system has cost savings of 43%-50%, and the cantilevered system has savings of 31%-40%. For a DIY prosumer the coupling of an open source EV charger kit with the racking designs provided here enable a grid-tied system for less than CAD$10,000. In addition, the curbside cantilever-based PV canopy opens up the potential for both property owners and municipalities to begin to offer on street PV-powered EV charging where there is on street parking. Including wood as a suitable material for potential PV parking canopies provides some additional value for increased material flexibility to overcome volatility of building materials costs.

The energy analysis performed for a single PV carport can be scaled to any number of solar carports. The energy produced by the proposed carport is compared to the needs of

Preprints (www.preprints.org) | NOT PEER-REVIEWED | Posted: 13 September 2022 doi:10.20944/preprints202209.0174.v1

North American Standards EV charging stations supplying multiple vehicles. Level 1 charging stations (1.4 kW) are the most compatible with a single PV carport whether the carport is in a residential area or at a workplace. When the carport is used with a level 3 charging station (50 kW or 100 kW), more than one carport is needed, and load sharing must be considered for an efficient charging of multiple EVs. In the specific case where the carport in connected to a net-metered grid and supplies a single EV, the annual energy generated by the PV is sufficient to power any EV currently in the market with an average annual mileage.

Supplementary Materials:

Author Contributions: Conceptualization, J.M.P.; methodology, N.V., K.S.H.; software, K.S.H.; validation, N.V., K.S.H.; formal analysis, J.M.P., N.V., K.S.H.; investigation, N.V., K.S.H.; resources, J.M.P.; data curation, N.V., K.S.H.; writing—original draft preparation J.M.P., N.V., K.S.H.; writing—review and editing, J.M.P., N.V., K.S.H.; visualization, N.V., K.S.H.; supervision, J.M.P.; funding acquisition, J.M.P.

Funding: This research was funded by Thompson Endowment.

Data Availability Statement: Data will be made available upon request.

Conflicts of Interest: The authors declare no conflict of interest. The funders had no role in the design of the study; in the collection, analyses, or interpretation of data; in the writing of the manuscript, or in the decision to publish the results.

Appendix A: Structural Analysis

Following the process outlined in [46], the factored design load for this canopy system in London Ontario is 2.27 kPa.

Once a design load based on location is calculated, the analysis outlined below can be followed. It is recommended to use an open source free beam calculator from ClearCalcs [86] to find critical structural values of complex members where analytical equations cannot be used.

The design load is assumed to be distributed evenly throughout the surface of the modules. Ensure that the modules being used have a higher structural capacity than the calculated design load. The load is then transferred from the panels to the joists. The design load is converted into a uniform distributed load onto each joist by multiplying the design load by the tributary width of each member, which in this case, is 1 m for inside joists, and 0.5 m for outside joists. This is denoted as w_f.

Single-Span System Analysis

The joists serve as a simply supported beam with two cantilevered ends as shown in Figure A1.

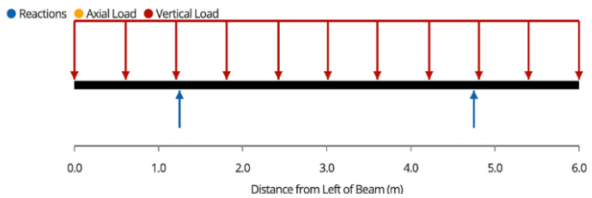

Figure A1. Single Span Joist Free Body Diagram

The shear force, bending moment, and deflection diagrams are qualitatively drawn in Figure A2a, 2b, and 2c below.

Preprints (www.preprints.org) | NOT PEER-REVIEWED | Posted: 13 September 2022 doi:10.20944/preprints202209.0174.v1

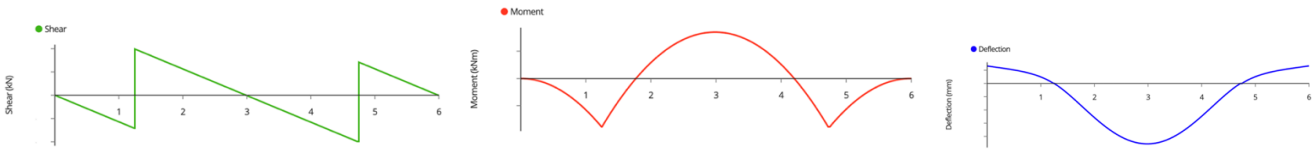

a) b) c)

Figure A2. Joist a) shear force diagram, b) bending moment diagram, and c) deflection diagram

The joists' maximum structural values can be solved analytically using the equations in Table A1. The values for the design load of 2.27 kPa are provided.

Table A1. Single-Span Joist Load Table for London Ontario

Maximum Component	Equation	Value
Reaction	$\frac{w_f L}{2}$	6.81 kN
Shear	$\frac{w_f L}{2} - w_f L_{Cant}$	3.97 kN
Moment	$\frac{w_f {L_{Cant}}^2}{2}$	1.77 kNm
Deflection	$\frac{5w{L_{Span}}^4}{384EI} - \frac{w{L_{Cant}}^2{L_{Span}}^2}{16EI}$	3.05 mm

Where L is the full length of the joist, L_{span} is the length between the support reactions, L_{cant} is the length overhanging cantilever end, E is the Young's Modulus of Wood, and I is the strong axis moment of inertia of the joist.

The load is then transferred to the beam, which can be accurately depicted as a continuous beam in Figure A3 with a uniform distributed load to serve as the beam's self-weight, and a series of point loads to serve as the joist reactions.

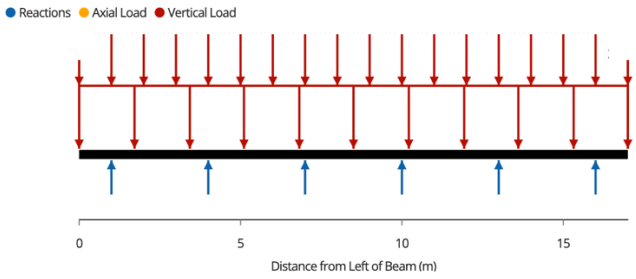

Figure A3. Continuous Beam Free Body Diagram

The shear force, bending moment, and deflection diagrams are qualitatively drawn in Figure A4a, 4b, and 4c below.

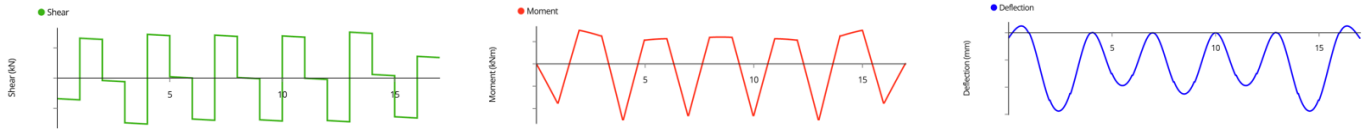

a) b) c)

Figure A4. Beam a) shear force diagram, b) bending moment diagram, and c) deflection diagram

This indeterminate beam can be solved using analytical methods such as the moment distribution method but solving analytically can be long and tedious. It is suggested to use

Preprints (www.preprints.org) | NOT PEER-REVIEWED | Posted: 13 September 2022 doi:10.20944/preprints202209.0174.v1

an open source beam calculator from Clear-Calcs [86] to quickly acquire these values. The results for London Ontario are summarized in Table A2.

Table A2. Single-Span Beam Load Table for London Ontario

Maximum Component	Value
Reaction	21.70 kN
Shear	7.61 kN
Moment	5.00 kNm
Deflection	1.44 mm

After the beam, the load is taken to the posts. The eccentricity between the center of the post and the beam should be taken into consideration to account for extra bending moment as seen in Figure A5.

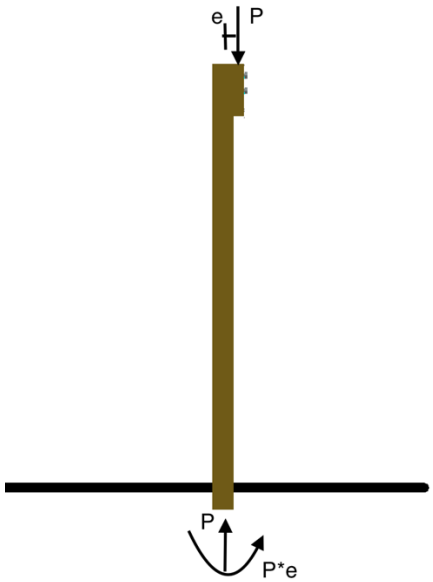

Figure A5. Single-Span Post Free Body Diagram with eccentric loading

P represents the reaction force carried from the beam to the post, and e is the distance between the center of the post and the center of the beam. Since this post is experience combined compression and bending, Equation A1, provided from the National Design Specification for Wood Construction [52], must be checked.

$$\frac{P}{fc^*} + \frac{P * e}{fb^*} \leq 1.00 \quad \text{(A1)}$$

Where *fc** is the compressive strength capacity of the post, and *fb** is the bending strength capacity. For a design load of 2.27 kPa on 6 x 6 posts, the combination of compression and bending is 0.92, which is adequate for this build.

A finite element analysis, described in Figure A6, can also be conducted to quickly calculate the stress of each member, where no members are overloaded.

Preprints (www.preprints.org) | NOT PEER-REVIEWED | Posted: 13 September 2022 doi:10.20944/preprints202209.0174.v1

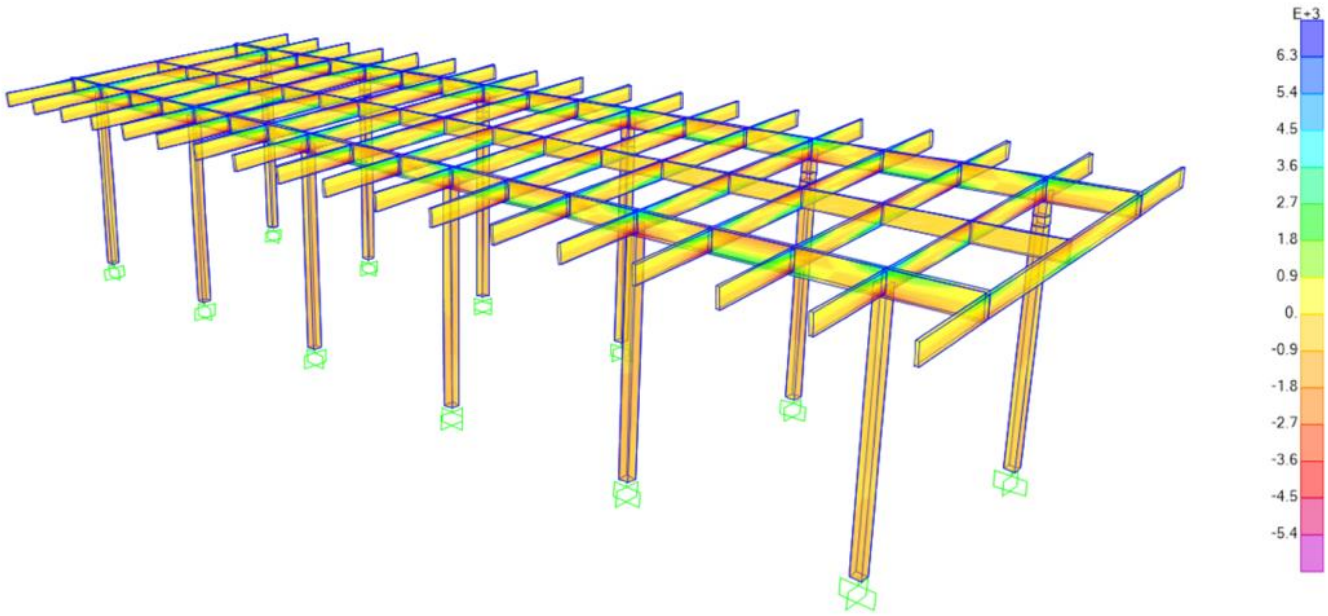

Figure A6. Stress contour of the Single-Span System with a finite element analysis.

Double-Span System Structural Analysis

The joists in this system exhibit the same results as they do in the single span system. The beams now have double the span length shown in Figure A7.

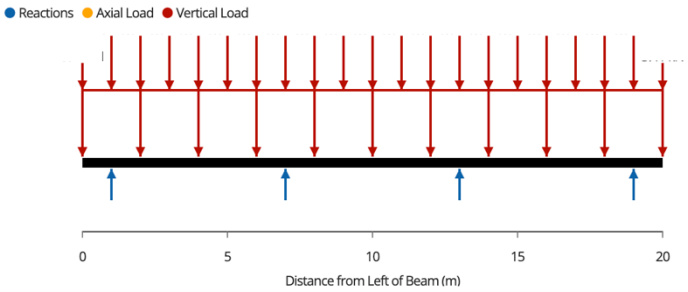

Figure A7. Double-Span Beam Free Body Diagram

The shear force, bending moment, and deflection diagrams are qualitatively drawn in Figure A8a, 4b, and 4c below.

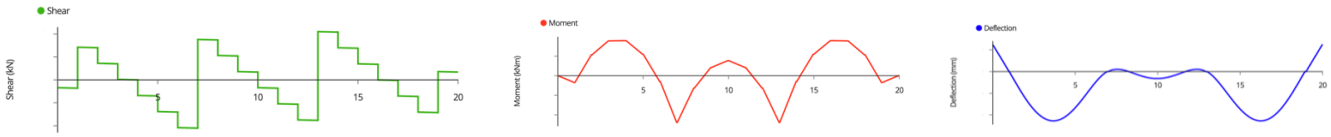

a) b) c)

Figure A8. Two-Span Beam a) shear force diagram, b) bending moment diagram, and c) deflection diagram

Preprints (www.preprints.org) | NOT PEER-REVIEWED | Posted: 13 September 2022 doi:10.20944/preprints202209.0174.v1

Using an open-source beam calculator, the results for a design load of 2.27 kPa are summarized in Table A3.

Table A3. Double-Span Beam Load Table for 2.27 kPa.

Maximum Component	Value
Reaction	45.50 kN
Shear	21.00 kN
Moment	23.90 kNm
Deflection	27.07 mm

The posts are analyzed in the same way as the single span system, but since the aluminum beam sits directly on the posts, need to consider eccentric loading, and thus the second component of the equation can be ignored.

A finite element analysis, described in Figure A9, can also be conducted to quickly calculate the stress of each member, where no members are overloaded.

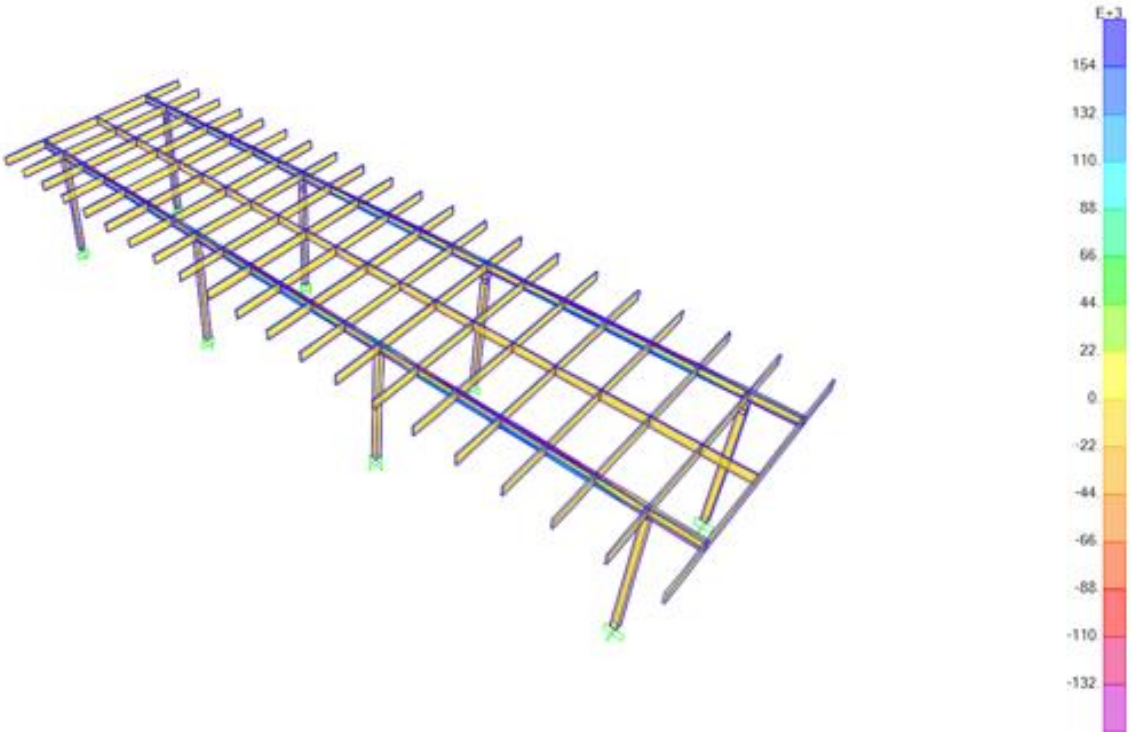

Figure A9. Double-Span System Stress Contour using finite element analysis

Cantilever System Analysis

The joists of the cantilever system exhibit the loading described in the free body diagram in Figure A10.

Preprints (www.preprints.org) | NOT PEER-REVIEWED | Posted: 13 September 2022 doi:10.20944/preprints202209.0174.v1

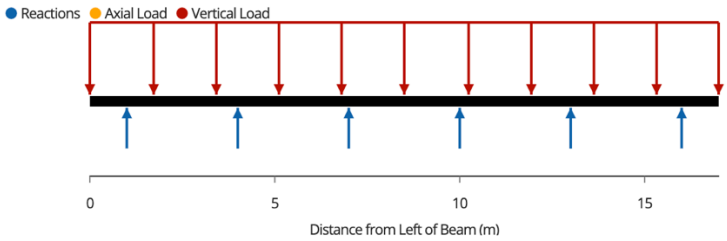

Figure A10. Cantilevered System Joists Free Body Diagram

The shear force, bending moment, and deflection diagrams are qualitatively drawn in Figure A11a, 4b, and 4c below.

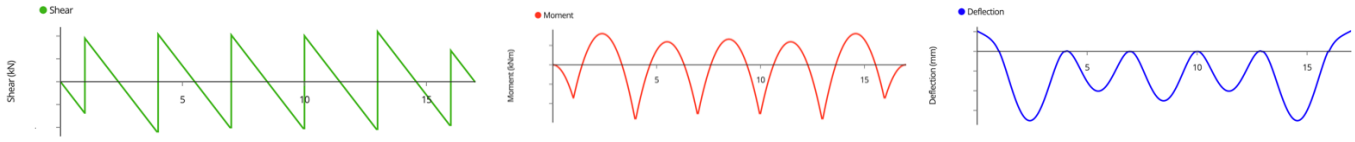

a) b) c)

Figure A11. Cantilever Joists a) shear force diagram, b) bending moment diagram, and c) deflection diagram

Using an open-source beam calculator, the results for a design load of 2.27 kPa are summarized in Table A4.

Table A4. Cantilevered System Joist Load Table for Design Load 2.27 kPa.

Maximum Component	Value
Reaction	7.11 kN
Shear	3.64 kN
Moment	1.85 kNm
Deflection	1.90 mm

The load is then transferred to the aluminum beams with the free body diagram described in Figure A12. The aluminum beams carry 5-point loads from the joists, and a uniform distributed load representing its self-weight. Beams are supported by a post, and is pulled down by the steel cable.

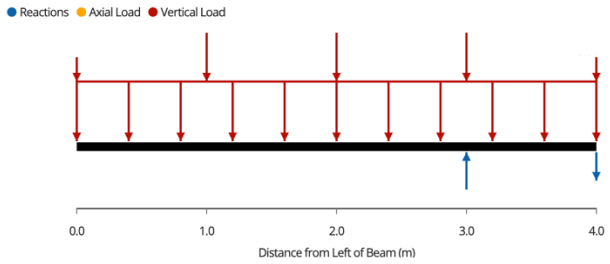

Figure A12. Cantilevered System Beam Free Body Diagram

The shear force, bending moment, and deflection diagrams are qualitatively drawn in Figure A13a, 4b, and 4c below.

Preprints (www.preprints.org) | NOT PEER-REVIEWED | Posted: 13 September 2022 doi:10.20944/preprints202209.0174.v1

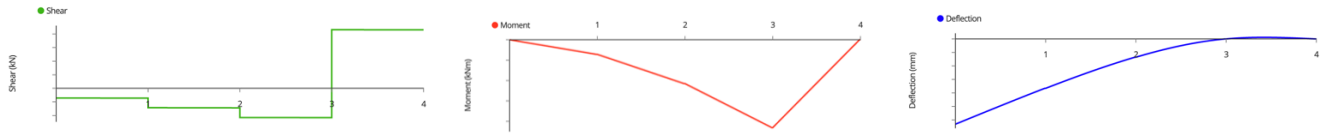

a) b) c)

Figure A13. Cantilever Beam a) shear force diagram, b) bending moment diagram, and c) deflection diagram

The beam can be analytically solved with the equations shown in Table A5.

Table A5. Cantilevered System Beam Load Table for Design Load 2.27 kPa.

Maximum Component	Equation	Value
Post Reaction	$8Reaction_{Joist} + 2w_{ow}L$	57.70 kN
Cable Tension	$4Reaction_{Joist} + w_{ow}L$	28.80 kN
Shear	$\sum Reaction_{Joist} + w_{ow}L_{Cant}$	32.50 kN
Moment	$\sum Reaction_{Joist} * x + w_{ow}\frac{{L_{Cant}}^2}{2}$	32.40 kNm
Deflection	$\frac{\sum Reaction_{Joist} * x^2(3L_{Cant}-x)}{6EI}$ [1]	60.30 mm

[1] This is an approximate equation but computes a result within 5% of the true value.

w_{ow} represents the uniform distributed own weight of the beam, $Reaction_{Joist}$ represents the reaction force found in Table A4, and x represents the distance between each reaction to the post.

Galvanized aircraft cable is recommended for the back support of the cantilever system. The size of cable can be selected by choosing the size with sufficient breaking strength against tensile loads [87]. For London Ontario, 1/4" 7 x 19 strand wire is adequate to carry the load.

A finite element analysis, described in Figure A14, can also be conducted to quickly calculate the stress of each member, where no members are overloaded.

Preprints (www.preprints.org) | NOT PEER-REVIEWED | Posted: 13 September 2022 doi:10.20944/preprints202209.0174.v1

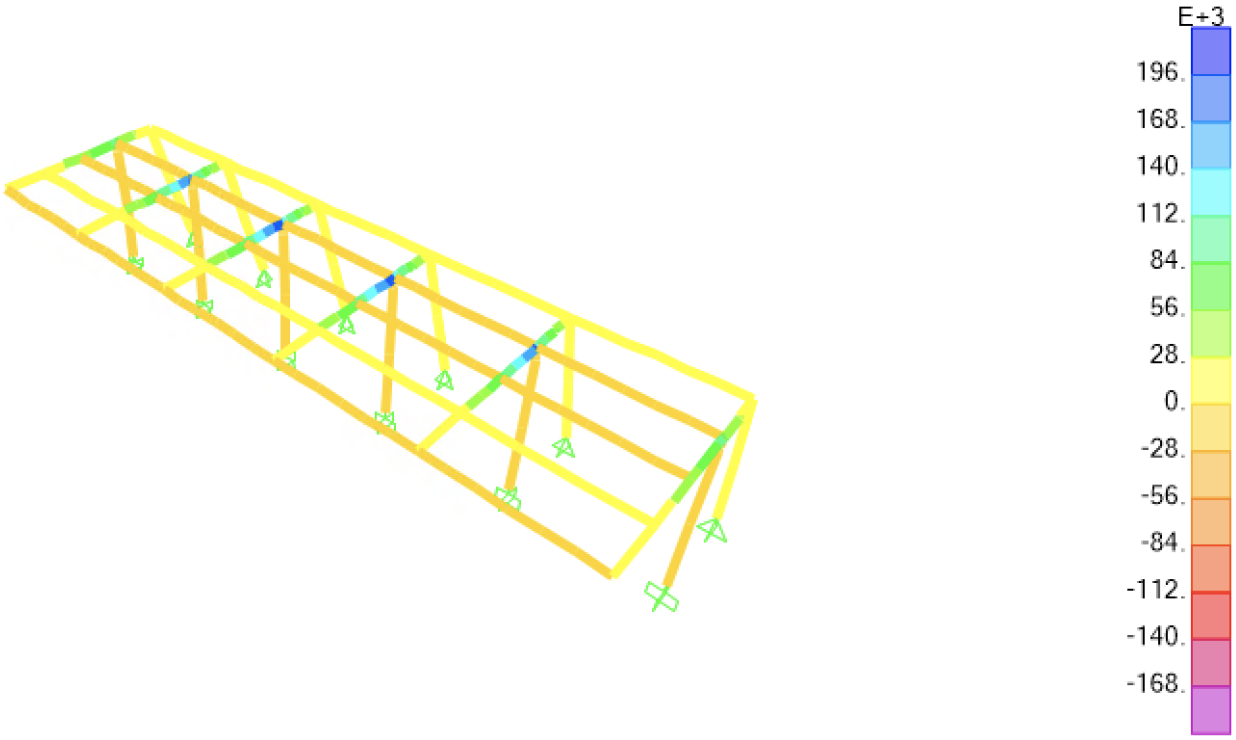

Figure A9. Cantilevered System Stress Contour using finite element analysis

The size of the concrete footing is dependent on the bearing capacity of the soil. This can easily be found using Table A6, extrapolated from NBCC Table 9.4.4.1 [51].

Table A6. Maximum Allowable Bearing Capacity for various soils as per the NBCC.

Soil Type and Condition	Value [kPa]
Dense Sand or Gravel	150
Loose Sand or Gravel	50
Dense Silt	100
Stiff Clay	150
Firm Clay	75
Soft Clay	40
Till	200
Clay Shale	300
Sound Rock	500

According to the NBCC, sand or gravel can be identified by a picket test in which a 38 mm by 38 mm picket beveled at the end at 45° to a point is pushed into the soil. The soil is then classified as dense if someone of average weight cannot push the picket more than 200 mm into the soil, and loose if the picket penetrates 200 mm or more. For clay and silt, stiff classification is denoted if it is difficult to indent by thumb pressure, firm classification is denoted if it can be indented by moderate thumb pressure, and soft classification is denoted if it can be easily penetrated by thumb pressure, where this test is carried out on undisturbed soil in the wall of a test pit.

It should be noted that these bearing capacity values provided by NBCC are conservative and may result in designing a footing significantly larger than what is required. If users desire, a geotechnical analysis can be conducted to find an accurate bearing capacity for their soil to design optimized footing sizes, but this service is subject to high engineering consulting costs.

Preprints (www.preprints.org) | NOT PEER-REVIEWED | Posted: 13 September 2022 doi:10.20944/preprints202209.0174.v1

Once a bearing capacity is found, the required footing diameter (d_f) for each post is calculated using Equation A2,

$$d_f = \sqrt{\frac{4 * P_L}{\pi * B_c}} \quad \text{(B2)}$$

Where Bc is the bearing capacity from Table B6 and P_L is the post load. The footings should be filled with 30 MPa concrete or other structural mixes to ensure sufficient durability against freeze-thaw cycles [88]. For locations in which freeze-thaw cycles are not critical, a 20 MPa mix can be used, and can be made simply by adding more water to the mix [88].

Appendix B: Modelling Parameters for Solar PV in SAM

The modelling parameters implemented into SAM have been summarized in Table B1.

Table B1. Modelling Parameters for Solar PV in SAM.

Parameters	Value	Source
System Type	Residential / No Economic Model	This Study
PV Module	LG Electronics Inc. LG410N2C-A5	
Efficiency	20.51%	
Length	2 m	[89]
Width	1 m	
Module Type	Mono Crystalline Silicon - Monofacial	
Number of Modules	15	This Study
Tilt Angle	5° (design requirement)	This Study
Azimuth	180°	This Study
DC Power Rating	6.154 kW_{DC}	This Study
DC to AC Ratio	1.02	This Study
Soiling Losses	5 %	
DC Power Losses	4.44 %	[55]
AC Power Losses	1 %	

References

1. Pearce, J. Photovoltaics - a Path to Sustainable Futures. *Futures* **2002**, *34*, 663–674, doi:10.1016/S0016-3287(02)00008-3.
2. Fu, R.; Feldman, D.; Margolis, R. U.S. Solar Photovoltaic System Cost Benchmark: Q1 2018. *Renew. Energy* **2018**, 63.
3. Dudley, D. Renewable Energy Will Be Consistently Cheaper Than Fossil Fuels By 2020, Report Claims Available online: https://www.forbes.com/sites/dominicdudley/2018/01/13/renewable-energy-cost-effective-fossil-fuels-2020/ (accessed on 29 August 2022).
4. Vaughan, A.; correspondent, A.V.E. Time to Shine: Solar Power Is Fastest-Growing Source of New Energy. *The Guardian* 2017.
5. Short-Term Energy Outlook - U.S. Energy Information Administration (EIA) Available online: https://www.eia.gov/outlooks/steo/report/electricity.php (accessed on 29 August 2022).
6. Global EV Outlook 2019 – Analysis - IEA Available online: https://www.iea.org/reports/global-ev-outlook-2019 (accessed on 29 August 2022).

Preprints (www.preprints.org) | NOT PEER-REVIEWED | Posted: 13 September 2022 doi:10.20944/preprints202209.0174.v1

7. Electric Revolution: As EV Demand Increases, Can Utilities and Cities Keep Up? Available online: https://www.utilitydive.com/news/electric-revolution-as-ev-demand-increases-can-utilities-and-cities-keep/564585/ (accessed on 29 August 2022).
8. 2019 Was the Year Electric Cars Grew up — Quartz Available online: https://qz.com/1762465/2019-was-the-year-electric-cars-grew-up/ (accessed on 29 August 2022).
9. EVO Report 2022 | BloombergNEF | Bloomberg Finance LP. *BloombergNEF*.
10. Vaughan, A. Renewable Energy Will Be World's Main Power Source by 2040, Says BP. *The Guardian* 2019.
11. Ong, S.; Campbell, C.; Denholm, P.; Margolis, R.; Heath, G. *Land-Use Requirements for Solar Power Plants in the United States*; 2013; p. NREL/TP-6A20-56290, 1086349;
12. Wiginton, L.K.; Nguyen, H.T.; Pearce, J.M. Quantifying Rooftop Solar Photovoltaic Potential for Regional Renewable Energy Policy. *Comput. Environ. Urban Syst.* **2010**, *34*, 345–357, doi:10.1016/j.compenvurbsys.2010.01.001.
13. Nguyen, H.T.; Pearce, J.M. Automated Quantification of Solar Photovoltaic Potential in Cities. *Int. Rev. Spat. Plan. Sustain. Dev.* **2013**, *1*, 49–60, doi:10.14246/irspsd.1.1_49.
14. Nguyen, H.T.; Pearce, J.; Harrap, R.; Barber, G. The Application of LiDAR to Assessment of Rooftop Solar Photovoltaic Deployment Potential in a Municipal District Unit. *Sensors* **2012**, *12*, 4534–4558, doi:10.3390/s120404534.
15. Heinstein, P.; Ballif, C.; Perret-Aebi, L.-E. Building Integrated Photovoltaics (BIPV): Review, Potentials, Barriers and Myths. *Green* **2013**, *3*, 125–156, doi:10.1515/green-2013-0020.
16. Biyik, E.; Araz, M.; Hepbasli, A.; Shahrestani, M.; Yao, R.; Shao, L.; Essah, E.; Oliveira, A.C.; del Caño, T.; Rico, E.; et al. A Key Review of Building Integrated Photovoltaic (BIPV) Systems. *Eng. Sci. Technol. Int. J.* **2017**, *20*, 833–858, doi:10.1016/j.jestch.2017.01.009.
17. Duke, R.; Williams, R.; Payne, A. Accelerating Residential PV Expansion: Demand Analysis for Competitive Electricity Markets. *Energy Policy* **2005**, *33*, 1912–1929, doi:10.1016/j.enpol.2004.03.005.
18. Denholm, P.; Margolis, R. Land-Use Requirements and the per-Capita Solar Footprint for Photovoltaic Generation in the United States. *Energy Policy* **2008**, *36*, 3531–3543, doi:10.1016/j.enpol.2008.05.035.
19. Krishnan, R.; Haselhuhn, A.; Pearce, J.M. Technical Solar Photovoltaic Potential of Scaled Parking Lot Canopies: A Case Study of Walmart U.S.A. *J. Innov. Sustain. RISUS* **2017**, *8*, 104–125, doi:10.24212/2179-3565.2017v8i2p104-125.
20. Alghamdi, A.; Bahaj, A.; Wu, P. Assessment of Large Scale Photovoltaic Power Generation from Carport Canopies. *Energies* **2017**, *10*, 686, doi:10.3390/en10050686.
21. Iringová, A.; Kovačic, M. Design and Optimization of Photovoltaic Systems in a Parking Garage - a Case Study. *Transp. Res. Procedia* **2021**, *55*, 1171–1179, doi:10.1016/j.trpro.2021.07.097.
22. Design and Optimization of Solar Carport Canopies for Maximum Power Generation and Efficiency at Bahawalpur Available online: https://search.emarefa.net/en/detail/BIM-1167304-design-and-optimization-of-solar-carport-canopies-for-maximu (accessed on 29 August 2022).
23. (8) (PDF) Performance and Analysis of Retail Store-centered Microgrids with Solar Photovoltaic Parking Lot, Cogeneration, and Battery-based Hybrid Systems Available online: https://www.researchgate.net/publication/351369632_Performance_and_analysis_of_retail_store-centered_microgrids_with_solar_photovoltaic_parking_lot_cogeneration_and_battery-based_hybrid_systems (accessed on 29 August 2022).
24. Deshmukh, S.; Pearce, J. Electric Vehicle Charging Potential from Retail Parking Lot Solar Photovoltaic Awnings. *Renew. Energy* **2021**, *169*, doi:10.1016/j.renene.2021.01.068.
25. Bhatti, A.R.; Salam, Z.; Aziz, M.J.B.A.; Yee, K.P. A Comprehensive Overview of Electric Vehicle Charging Using Renewable Energy. *Int. J. Power Electron. Drive Syst. IJPEDS* **2016**, *7*, 114.
26. *Solar Powered Charging Infrastructure for Electric Vehicles: A Sustainable Development*; Erickson, L.E., Robinson, J., Brase, G., Cutsor, J., Eds.; CRC Press, Taylor & Francis Group: Boca Raton, 2017; ISBN 978-1-4987-3156-0.

Preprints (www.preprints.org) | NOT PEER-REVIEWED | Posted: 13 September 2022 doi:10.20944/preprints202209.0174.v1

27. Nunes, P.; Figueiredo, R.; Brito, M.C. The Use of Parking Lots to Solar-Charge Electric Vehicles. *Renew. Sustain. Energy Rev.* **2016**, *66*, 679–693, doi:10.1016/j.rser.2016.08.015.
28. Chandra Mouli, G.R.; Bauer, P.; Zeman, M. System Design for a Solar Powered Electric Vehicle Charging Station for Workplaces. *Appl. Energy* **2016**, *168*, 434–443, doi:10.1016/j.apenergy.2016.01.110.
29. Analysis of Energy Capture by Vehicle Solar Roofs in Conjunction | PDF | Photovoltaics | Solar Power Available online: https://www.scribd.com/document/445304827/Analysis-of-energy-capture-by-vehicle-solar-roofs-in-conjunction (accessed on 29 August 2022).
30. Kempton, W.; Tomić, J. Vehicle-to-Grid Power Fundamentals: Calculating Capacity and Net Revenue. *J. Power Sources* **2005**, *144*, 268–279, doi:10.1016/j.jpowsour.2004.12.025.
31. Kempton, W.; Tomić, J. Vehicle-to-Grid Power Implementation: From Stabilizing the Grid to Supporting Large-Scale Renewable Energy. *J. Power Sources* **2005**, *144*, 280–294, doi:10.1016/j.jpowsour.2004.12.022.
32. Sortomme, E.; El-Sharkawi, M. Optimal Charging Strategies for Unidirectional Vehicle-to-Grid. *Smart Grid IEEE Trans. On* **2011**, *2*, 131–138, doi:10.1109/TSG.2010.2090910.
33. Chunhua, L.; Chau, K.T.; Wu, D.; Gao, S. Opportunities and Challenges of Vehicle-to-Home, Vehicle-to-Vehicle, and Vehicle-to-Grid Technologies. *Proc. IEEE* **2013**, *101*, 2409–2427, doi:10.1109/JPROC.2013.2271951.
34. (8) Optimal Integration of a Hybrid Solar-Battery Power Source into Smart Home Nanogrid with Plug-in Electric Vehicle | Request PDF Available online: https://www.researchgate.net/publication/318831345_Optimal_integration_of_a_hybrid_solar-battery_power_source_into_smart_home_nanogrid_with_plug-in_electric_vehicle (accessed on 29 August 2022).
35. Fathabadi, H. Novel Solar Powered Electric Vehicle Charging Station with the Capability of Vehicle-to-Grid. *Sol. Energy* **2017**, *142*, 136–143, doi:10.1016/j.solener.2016.11.037.
36. M, T.W., Krishnamurthy M. ,Jiang Y. ,Shahidehpour ["Vehicle Charging Stations with Solar Canopy: A Realistic Case Study within a Smart Grid Environment"] Available online: https://sciexplore.ir/Documents/Details/648-833-223-614 (accessed on 29 August 2022).
37. Lee, S.; Iyengar, S.; Irwin, D.; Shenoy, P. Shared Solar-Powered EV Charging Stations: Feasibility and Benefits. In Proceedings of the 2016 Seventh International Green and Sustainable Computing Conference (IGSC); IEEE: Hangzhou, China, 2016; pp. 1–8.
38. Kootenay Steel & Wood Carport Available online: https://grizzlyshelter.ca/products/kootenay-steel-metal-and-wood-carport (accessed on 17 August 2022).
39. Kootenay 2 Post Steel and Wood Carport Available online: https://grizzlyshelter.ca/products/kootenay-2-post-cantilever-carport (accessed on 17 August 2022).
40. Sunjoy AutoCove 20 Ft. x 11 Ft. Hanover Cedar Wood Carport - Wayfair Canada Available online: https://www.wayfair.ca/Sunjoy--AutoCove-20-ft.-x-11-ft.-Hanover-Cedar-Wood-Carport-A110000900-L623-K~LKJP3376.html?refid=GX185556028987-LKJP3376&device=c&ptid=1339009412562&targetid=aud-835011428576:pla-1339009412562&network=g&ireid=212428809&gclid=CjwKCAjwo_KXBhAaEiwA2RZ8hHXImEHNr-qAC9BYXj0CYJNtn2YxljAk4m4FTPTuhSZOHPi7UZhoTlxoCaF8QAvD_BwE (accessed on 17 August 2022).
41. Domestic Solar Carport by Polysolar Available online: https://www.specifiedby.com/polysolar/domestic-solar-carport (accessed on 17 August 2022).
42. Miller, C. General Motors Will Launch Electric Heavy-Duty Trucks by 2035 Available online: https://www.caranddriver.com/news/a38696855/general-motors-electric-heavy-duty-trucks/ (accessed on 29 August 2022).
43. Solar Carport. *Polar Rack.*
44. 6512.17C$ 40% OFF|2 Parking Space 5kw Carport Solar System For Home - Instrument Parts & Accessories - AliExpress Available online:

Preprints (www.preprints.org) | NOT PEER-REVIEWED | Posted: 13 September 2022 doi:10.20944/preprints202209.0174.v1

//www.aliexpress.com/item/1005004384076086.html?src=ibdm_d03p0558e02r02&sk=&aff_platform=&aff_trace_key=&af=&cv=&cn=&dp= (accessed on 18 August 2022).

45. Polivchuk, J. Exploring the Feasibility and Costs and Benefits of Solar Carports for the Calgary Parking Authority. **2018**.
46. Vandewetering, N.; Hayibo, K.S.; Pearce, J.M. Impacts of Location on Designs and Economics of DIY Low-Cost Fixed-Tilt Open Source Wood Solar Photovoltaic Racking. *Designs* **2022**, *6*, 41, doi:10.3390/designs6030041.
47. Vandewetering, N.; Hayibo, K.S.; Pearce, J.M. Open-Source Design and Economics of Manual Variable-Tilt Angle DIY Wood-Based Solar Photovoltaic Racking System. *Designs* **2022**, *6*, 54, doi:10.3390/designs6030054.
48. Lehmann, S. Sustainable Construction for Urban Infill Development Using Engineered Massive Wood Panel Systems. *Sustainability* **2012**, *4*, 2707–2742, doi:10.3390/su4102707.
49. Amiri, A.; Ottelin, J.; Sorvari, J.; Junnila, S. Cities as Carbon Sinks—Classification of Wooden Buildings. *Environ. Res. Lett.* **2020**, *15*, 094076, doi:10.1088/1748-9326/aba134.
50. Embodied Carbon Footprint Database. *Circ. Ecol.*
51. *National Building Code of Canada 2015*; National Research Council of Canada, Ed.; NRCC; Fourteenth edition.; National Research Council of Canada: Ottawa, 2015; ISBN 978-0-660-03633-5.
52. 2018 NDS Available online: https://awc.org/publications/2018-nds/ (accessed on 8 March 2022).
53. Aluminum Beam 6061 Available online: https://www.metalsupermarkets.com/product/aluminum-beam-6061/ (accessed on 10 August 2022).
54. CSA S157.1-05 Alumninum Design Code (1) - Free Download PDF Available online: https://kupdf.net/download/csa-s157-1-05-alumninum-design-code-1_58e2f8b6dc0d60470dda97e4_pdf (accessed on 11 August 2022).
55. Freeman, J.M.; DiOrio, N.A.; Blair, N.J.; Neises, T.W.; Wagner, M.J.; Gilman, P.; Janzou, S. *System Advisor Model (SAM) General Description (Version 2017.9.5)*; National Renewable Energy Lab. (NREL), Golden, CO (United States), 2018;
56. Milosavljević, D.D.; Kevkić, T.S.; Jovanović, S.J. Review and Validation of Photovoltaic Solar Simulation Tools/Software Based on Case Study. *Open Phys.* **2022**, *20*, 431–451, doi:10.1515/phys-2022-0042.
57. EV Database Available online: https://ev-database.org/ (accessed on 29 August 2022).
58. Falvo, M.C.; Sbordone, D.; Bayram, I.S.; Devetsikiotis, M. Ev Charging Stations and Modes: International Standards. In Proceedings of the in Proc. IEEE International Symposium on Power Electronics, Electrical Drives, Automation and Motion; 2014.
59. Assessment of Electric Vehicles Concerning Impacts, Charging Infrastructure with Unidirectional and Bidirectional Chargers, and Power Flow Comparisons - Habib - 2018 - International Journal of Energy Research - Wiley Online Library Available online: https://onlinelibrary.wiley.com/doi/10.1002/er.4033 (accessed on 29 August 2022).
60. Li, Y.; Hu, J.; Chen, F.; Liu, S.; Yan, Z.; He, Z. A New-Variable-Coil-Structure-Based IPT System With Load-Independent Constant Output Current or Voltage for Charging Electric Bicycles. *IEEE Trans. Power Electron.* **2018**, *33*, 8226–8230, doi:10.1109/TPEL.2018.2812716.
61. Chen, Y.; Zhang, H.; Park, S.-J.; Kim, D.-H. A Switching Hybrid LCC-S Compensation Topology for Constant Current/Voltage EV Wireless Charging. *IEEE Access* **2019**, *7*, 133924–133935, doi:10.1109/ACCESS.2019.2941652.
62. Daily Electric Vehicle Charging Load Profiles Considering Demographics of Vehicle Users - ScienceDirect Available online: https://www.sciencedirect.com/science/article/pii/S0306261920305754?via%3Dihub (accessed on 29 August 2022).
63. Average KMs Driven Per Year | How Much Do Canadians Drive? Available online: https://www.thinkinsure.ca/insurance-help-centre/average-km-per-year-canada.html (accessed on 9 September 2022).
64. EV Database Available online: https://ev-database.org/cheatsheet/energy-consumption-electric-car (accessed on 9 September 2022).

65. Sadat, S.A.; Vandewetering, N.; Pearce, J.M. Mechanical and Economic Analysis of Conventional Aluminum Photovoltaic Module Frames, Frames with Side Holes, and Open-Source Downward-Fastened Frames for Non-Traditional Racking. *Be Publ.*
66. Lumber - 2022 Data - 1978-2021 Historical - 2023 Forecast - Price - Quote - Chart Available online: https://tradingeconomics.com/commodity/lumber (accessed on 26 July 2022).
67. Aluminum - 2022 Data - 1989-2021 Historical - 2023 Forecast - Price - Quote - Chart Available online: https://tradingeconomics.com/commodity/aluminum (accessed on 26 July 2022).
68. Top 10 Aluminum-Producing Countries (Updated 2022) Available online: https://investingnews.com/daily/resource-investing/industrial-metals-investing/aluminum-investing/aluminum-producing-countries/ (accessed on 18 August 2022).
69. Raw Aluminium | OEC Available online: https://oec.world/en/profile/hs/raw-aluminium (accessed on 17 August 2022).
70. New Energy Vehicle Solar Charging Station Wallbox 22Kw Ev Station Ev Battery Charger For Home Use With Mppt Photovoltaic Panels| | - AliExpress Available online: https://www.aliexpress.com/item/1005004354876999.html?spm=a2g0o.ppclist.product.2.519cxOEix-OEiQQ&pdp_npi=2%40dis%21CAD%21C%24%207%2C230.85%21C%24%207%2C230.85%21%21%21%21%21%402101f6b116607501899558239e7ffc%21120000028877238090%21btf&_t=pvid:d8a0fdbc-3dd2-4032-8f80-d6fe9ba25004&afTraceInfo=1005004354876999__pc__pcBridgePPC__xxxxxx__1660750190 (accessed on 17 August 2022).
71. Tamarack Solar Top of Pole Mounts for Large Solar Panels Available online: https://www.altestore.com/store/solar-panel-mounts/top-of-pole-mounts-for-solar-panels/tamarack-solar-top-of-pole-mounts-6072-cell-solar-panels-p40745/ (accessed on 18 August 2022).
72. TPM3 Pole Mount for Three 60/72 Cell Solar Modules Available online: https://www.off-the-grid-solar.com/products/tpm3-pole-mount-for-three-60-72-cell-solar-modules (accessed on 18 August 2022).
73. 12 Solar Panel Ground Mounting Kit IronRidge Available online: https://sunwatts.com/12-solar-panel-ground-mounting-kit-ironridge/ (accessed on 26 July 2022).
74. Hot Car Fatalities Are Year-Round Threat Available online: https://www.consumerreports.org/car-safety/hot-car-fatalities-year-round-threat-to-children-pets-heat-stroke-a2015990109/ (accessed on 29 August 2022).
75. Golden, J. Photovoltaic Canopies: Thermodynamics to Achieve a Sustainable Systems Approach to Mitigate the Urban Heat Island Hysteresis Lag Effect. *Int. J. Sustain. Energy* **2006**, *25*, 1–21, doi:10.1080/14786450600593139.
76. Golden, J.S.; Carlson, J.; Kaloush, K.E.; Phelan, P. A Comparative Study of the Thermal and Radiative Impacts of Photovoltaic Canopies on Pavement Surface Temperatures. *Sol. Energy* **2007**, *81*, 872–883, doi:10.1016/j.solener.2006.11.007.
77. OpenEVSE - Electric Vehicle Charging Solutions Available online: https://www.openevse.com/ (accessed on 29 August 2022).
78. Canadian Solar 340W Solar Panel | CS1H-340MS – Volts Energies Available online: https://volts.ca/products/canadian-solar-340w-solar-panel-cs1h-340ms?currency=CAD&utm_medium=product_sync&utm_source=google&utm_content=sag_organic&utm_campaign=sag_organic (accessed on 26 July 2022).
79. Shingled 680 Watt Solar Panel - Panneau Solaire 680w -All Black 340w Canadian Solar Panels With [CSA Approval], For RV, Boats, Cottages, Camping and All Off-Grid Applications (2) Available online: https://solarpowerstore.ca/products/made-in-canada-shingled-340-watt-solar-panel-panneau-solaire-340w-all-black-340w-canadian-solar-panels-with-csa-approval (accessed on 26 July 2022).

Preprints (www.preprints.org) | NOT PEER-REVIEWED | Posted: 13 September 2022 doi:10.20944/preprints202209.0174.v1

80. Canadian Solar Bi-Facial CS3W-435MB-AG Solar Panel – Volts Energies Available online: https://volts.ca/products/canadian-solar-bi-facial-445w-solar-panel-cs3w-445mb-ag?currency=CAD&utm_medium=product_sync&utm_source=google&utm_content=sag_organic&utm_campaign=sag_organic (accessed on 26 July 2022).
81. Canadian Solar - 335W, Monocrystalline Solar PV Module. *Raysolar Store*.
82. Canadian Solar - CS1Y-390MS, 390W Mono Perc Available online: https://www.off-the-grid-solar.com/products/canadian-solar-cs1y-390ms-390w-mono-perc (accessed on 26 July 2022).
83. Hess, D.J. The Politics of Niche-Regime Conflicts: Distributed Solar Energy in the United States. *Environ. Innov. Soc. Transit.* **2016**, *19*, 42–50, doi:10.1016/j.eist.2015.09.002.
84. Prehoda, E.; Pearce, J.M.; Schelly, C. Policies to Overcome Barriers for Renewable Energy Distributed Generation: A Case Study of Utility Structure and Regulatory Regimes in Michigan. *Energies* **2019**, *12*, 674, doi:10.3390/en12040674.
85. Lee, D.; Hess, D.J. Incumbent Resistance and the Solar Transition: Changing Opportunity Structures and Framing Strategies. *Environ. Innov. Soc. Transit.* **2019**, *33*, 183–195, doi:10.1016/j.eist.2019.05.005.
86. Free Beam Calculator | ClearCalcs Available online: https://clearcalcs.com/freetools/beam-analysis (accessed on 11 August 2022).
87. Galvanized Aircraft Cable 7x19, 1/4 in. x 200 Feet Available online: https://www.bestmaterials.com/detail.aspx?ID=25064 (accessed on 11 August 2022).
88. Kessy, J.G.; Alexander, M.G.; Beushausen, H. Concrete Durability Standards: International Trends and the South African Context. *J. South Afr. Inst. Civ. Eng.* **2015**, *57*, 47–58, doi:10.17159/2309-8775/2015/v57n1a5.
89. Lg LG410N2C-A5 Manuals | ManualsLib Available online: https://www.manualslib.com/products/Lg-Lg410n2c-A5-9238432.html (accessed on 29 August 2022).